AGU PUBLICATIONS

Tectonics

RESEARCH ARTICLE
10.1002/2015TC003869

Key Points:
- Active right lateral strike-slip tectonics affects the northern edge of Lut Block
- Tectonic fingerprint is deciphered from fault-related ridge geomorphic signal
- New insights on recent kinematic evolution in Central Iran are provided

Supporting Information:
- Texts S1 and S2 and Figures S1 and S2
- Table S1

Correspondence to:
M. Della Seta,
marta.dellaseta@uniroma1.it

Citation:
Calzolari, G., M. Della Seta, F. Rossetti, R. Nozaem, G. Vignaroli, D. Cosentino, and C. Faccenna (2016), Geomorphic signal of active faulting at the northern edge of Lut Block: Insights on the kinematic scenario of Central Iran, *Tectonics*, *35*, doi:10.1002/2015TC003869.

Received 23 FEB 2015
Accepted 28 OCT 2015
Accepted article online 8 NOV 2015

Geomorphic signal of active faulting at the northern edge of Lut Block: Insights on the kinematic scenario of Central Iran

Gabriele Calzolari[1], Marta Della Seta[2], Federico Rossetti[1], Reza Nozaem[3], Gianluca Vignaroli[4], Domenico Cosentino[1], and Claudio Faccenna[1]

[1]Dipartimento di Scienze, Università Roma Tre, Rome, Italy, [2]Dipartimento di Scienze della Terra, Sapienza Università di Roma, Rome, Italy, [3]Department of Geology, Imam Khomeini International University, Qazvin, Iran, [4]Istituto di Geologia Ambientale e Geoingegneria, CNR, Area della Ricerca di Roma 1, Rome, Italy

Abstract Recent works documented Neogene to Quaternary dextral strike-slip tectonics along the Kuh-e-Sarhangi and Kuh-e-Faghan intraplate strike-slip faults at the northern edge of the Lut Block of Central Iran, previously thought to be dominated by sinistral strike-slip deformation. This work focuses on the evidence of Quaternary activity of one of these fault systems, in order to provide new spatiotemporal constraints on their role in the active regional kinematic scenario. Through geomorphological and structural investigation, integrated with optically stimulated luminescence dating of three generations of alluvial fans and fluvial terraces (at ~53, ~25, and ~6 ka), this study documents (i) the topographic inheritance of the long-term (Myr) punctuated history of fault nucleation, propagation, and exhumation along the northern edge of Lut Block; (ii) the tectonic control on drainage network evolution, pediment formation, fluvial terraces, and alluvial fan architecture; (iii) the minimum Holocene age of Quaternary dextral strike-slip faulting; and (iv) the evidence of Late Quaternary fault-related uplift localized along the different fault strands. The documented spatial and temporal constraints on the active dextral strike-slip tectonics at the northern edge of Lut Block provide new insights on the kinematic model for active faulting in Central Iran, which has been reinterpreted in an escape tectonic scenario.

1. Introduction

In tectonically active regions the drainage network at the scale of single fault systems responds rapidly to fault-related topographic perturbations [*Jackson et al*., 1996; *Royden and Perron*, 2013; *Willett et al*., 2014], being sensitive to changes in the local base level of river erosion. The latter is directly controlled by local rock uplift/subsidence, which often causes drainage reorganization in transient landscapes [e.g., *Castelltort et al*., 2012; *Fubelli et al*., 2014]. On the other hand, at the scale of a single fault system the effects of climatic fluctuations, which normally influence the erosion/deposition dynamics, are generally uniform. Therefore, tectonic signals in the landscape can be recorded by geomorphic markers [*Burbank and Anderson*, 2012] and, in particular, fluvial terraces and alluvial fans [e.g., *Rockwell et al*., 1984; *Avouac et al*., 1993; *Schiattarella et al*., 2006; *Della Seta et al*., 2008; *Troiani and Della Seta*, 2008, 2011; *Wegmann and Pazzaglia*, 2009; *Gioia et al*., 2014; *Giano et al*., 2014]. In the case of strike-slip tectonics, active faulting is commonly documented through progressive rotation of streams across the fault zones [e.g., *Belisario et al*., 1999; *Della Seta et al*., 2004] and/or through the offset of stream channels and alluvial landforms [e.g., *Allen*, 1965; *Replumaz et al*., 2001; *Hubert-Ferrari et al*., 2002], the latter more frequently observed in arid regions [*Walker and Jackson*, 2002; *Foroutan et al*., 2014]. Nonetheless, the topographic growth of linear ridges associated with strike-slip fault systems can result in a more complex geomorphic response to active faulting [*Bull*, 2009], which may not be necessarily recorded in the proximity of the single fault segments.

Central Iran provides spectacular examples of narrow, topographically prominent linear ridges associated with active strike-slip fault systems. These fault systems developed in response to the Arabia-Eurasia plate convergence (Figure 1a), along inherited crustal anisotropies. The latter represent relict plate margin structures, incorporated during long-lasting continental collision and accretion processes, and bound a mosaic of continental blocks [*Aghanabati*, 2004], collectively named as Central East Iran Microcontinent (CEIM).

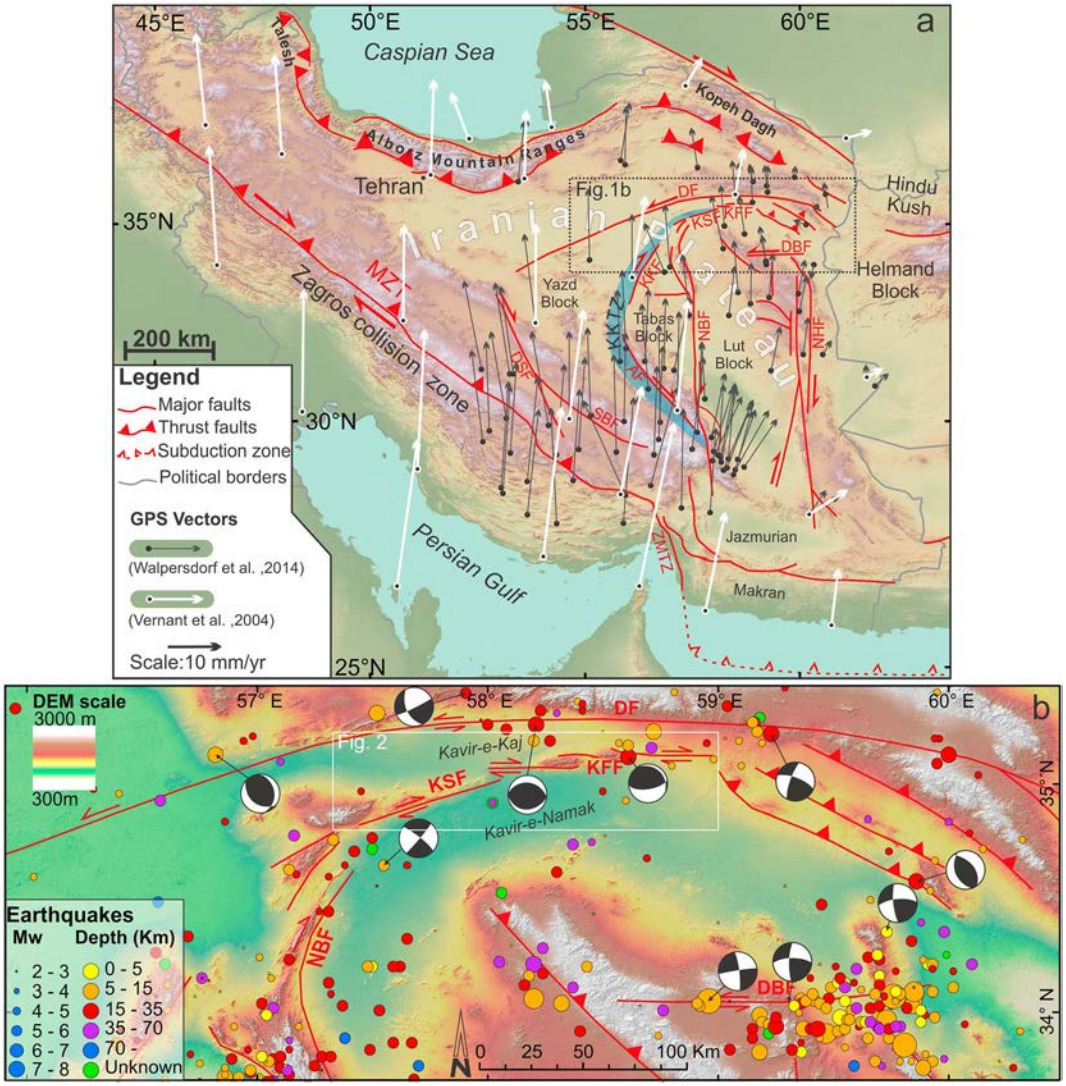

Figure 1. (a) Simplified tectonic map of Iran, showing the main collisional and intraplate strike-slip fault domains accommodating the Arabia-Eurasia convergence (modified after *Calzolari et al.* [2015]). DSF: Dehshir Fault; KKF: Kalmard-Kuhbanan Fault, DBF: Dasht-e-Bayaz Fault, KSF: Kuh-e-Sarhangi Fault; MZT: Main Zagros Trust; NBF: Nayband Fault; NHF: Nehbandan Fault; SBF: Shahr-e-Babak Fault; ZMTZ: Zagros-Makran Transfer Zone; KKTZ: Kashmar-Kerman Tectonic Zone. GPS velocities vectors in Iran relative to stable Eurasia are shown with different colors according to *Vernant et al.* [2004] and *Walpersdorf et al.* [2014]. (b) Simplified tectonic map of northern Central Iran, showing the historical and instrumental seismicity of the area. Focal mechanisms are taken from the Harvard catalog (http://www.globalcmt.org/CMTsearch.html). Epicenters are from the International Seismic Centre *EHB Bulletin* (Thatcham, UK, 2009, http://www.isc.ac.uk) and the earthquake catalog at Iranian Institute of Earthquake Engineering and Seismology (http://www.iiees.ac.ir). The white rectangle indicates the location of the study area and the extent of the map in Figure 2.

In the last decades, these fault systems have been incorporated into a scenario of dynamic rupture during the continuous N-S directed Arabia-Eurasia convergence, associated with rigid block rotations and strain partitioning along N-S dextral and E-W sinistral fault systems [e.g., *Allen et al.*, 2004; *Walker and Jackson*, 2004; *Mattei et al.*, 2012; *Walpersdorf et al.*, 2014]. However, Neogene to Quaternary dextral strike-slip deformation, not compatible with such a scenario, was recently documented along the NE-SW Kuh-e-Sarhangi Fault (KSF) [*Nozaem et al.*, 2013] and the E-W Kuh-e-Faghan Fault (KFF) [*Calzolari et al.*, 2015]. These new findings are particularly relevant since these fault systems developed to the south of the Doruneh Fault, which was previously thought to bound the northern termination of the CEIM (Figure 1). Significantly, *Javadi et al.* [2013, 2015] documented a kinematic reversal of the Doruneh Fault from dextral to sinistral in the late Neogene. This field evidence attests that the fault strands bounding the northern termination of

the CEIM were part of a distributed zone of Neogene dextral shear running from the Himalayan syntaxes to the Albortz range [*Javadi et al*., 2015].

In order to revise the existing kinematic scenario proposed for the CEIM, it is therefore essential to better constrain the spatiotemporal distribution and activity of dextral shearing along the northern termination of the CEIM. In fact, although the Neogene history of such fault systems was already documented [*Nozaem et al*., 2013; *Calzolari et al*., 2015; *Javadi et al*., 2015], the Quaternary and active deformation pattern is still poorly detailed and time constrained. Following a tectonic-geomorphological approach, in the light of the structural scenario described in *Nozaem et al*. [2013] and *Calzolari et al*. [2015] for the KSF and KFF systems, respectively, this study aims to provide new temporal and kinematic constraints to the neotectonic evolution of the northern edge of Lut Block to the south of the Doruneh Fault (Figure 1). In such a perspective, this study is conceived as a companion of *Calzolari et al*. [2015] and aims specifically (i) to outline the topographic inheritance of the long-term history of KFF fault nucleation, propagation, and exhumation; (ii) to identify the inherited and active tectonic fingerprint in drainage network evolution, pediment formation, fluvial terraces, and alluvial fan architecture; and (iii) to constrain the minimum age of Quaternary dextral fault activity and associated localized uplift. To accomplish these aims, we performed (i) topographic analyses; (ii) structural and geomorphological field surveys, integrated with satellite image interpretation; (iii) optically stimulated luminescence (OSL) dating of geomorphic markers; and (iv) statistical analysis of alluvial fan slope angles. The final purpose is to provide new constraints on active fault systems, which could help future revisions of the kinematic model of Central Iran.

2. Geological Background

The Arabia-Eurasia convergence culminated with continental collision at the Eocene-Oligocene boundary [e.g., *Jolivet and Faccenna*, 2000; *Homke et al*., 2010; *Agard et al*., 2011; *Mouthereau et al*., 2012], resulting in the late Cenozoic distribution of the Iranian region [*Hatzfeld and Molnar*, 2010]. Such convergence is still active, as testified by GPS velocity vectors, which indicate a NNE motion of the Arabian plate relative to Eurasia of ~25 mm/yr [*Sella et al*., 2002; *McClusky et al*., 2003; *Nilforoushan et al*., 2003; *Vernant et al*., 2004; *Reilinger et al*., 2006; *Walpersdorf et al*., 2014] (Figure 1). The convergence is mostly accommodated by major contractional belts bounding the Iranian Plateau [*Jackson et al*., 1995; *Talebian and Jackson*, 2002, 2004; *Allen et al*., 2004; *Walker and Jackson*, 2004; *Hatzfeld and Molnar*, 2010; *Madanipour et al*., 2013] (Figure 1): the Zagros to the southwest, and the Talesh, the Alborz, and the Kopeh Dagh north of 35°N. To the east, the CEIM consists of a mosaic of continental blocks (i.e., Yazd, Tabas, and Lut blocks [*Aghanabati*, 2004]), bounded by linear mountain belts developed along major strike-slip fault zones that have distinctive stratigraphy, deformation style, and pattern of recent seismicity [*Berberian and King*, 1981; *Berberian*, 2014]. Such strike-slip fault systems accommodate differential northward motion among the continental blocks that make up the CEIM, which, according to recently published GPS data, are moving northward at 6–13 mm/yr with respect to the stable Afghanistan [*Walpersdorf et al*., 2014] (Figure 1a). These fault systems are organized into N-S dextral (from west to east: the Deshir (DSF), Nayband (NBF) and Nehbandan (NHB) faults) and E-W sinistral (from north to south: Doruneh (DF) and Dasht-e-Bayaz (DBF) faults) shear zones (Figure 1a). Their kinematics and total cumulative offsets along their active segments have been detailed using both geological and displaced geomorphic markers from satellite imagery [*Walker and Jackson*, 2004; *Allen et al*., 2004, 2011; *Farbod et al*., 2011; *Foroutan et al*., 2014]. Taking into account the present-day slip rates (~2–10 mm/yr) along the major fault systems, the onset of strike-slip tectonics is inferred to date back to ~5 Ma, concurrent with the tectonic reorganization recognized throughout the Arabia-Eurasia convergence zone [e.g., *Allen et al*., 2004]. Destructive earthquakes occurred in Central Iran in recent years and the last century (e.g., Tabas in 1979, $M_s = 7.7$; Dasht-e-Bayaz in 1979, $M_w = 7.1$; and Bam 2003, $M_w = 6.5$), testifying to the high seismicity and active tectonics along these fault strands [*Hessami et al*., 2003].

The Tabas and Yazd blocks are separated by a nearly 600 km long, arcuate and structurally complex fault-bounded belt known as the Kashmar-Kerman Tectonic Zone (Figure 1), where remarkable exposures of the deeper sections (upper Neoproterozoic to lower Paleozoic in age) of the Central Iran basement occur [*Ramezani and Tucker*, 2003; *Rossetti et al*., 2015]. *Nozaem et al*. [2013] proposed that the dextral strike-slip KSF represents the Neogene to Quaternary tectonic reactivation of the Kashmar-Kerman Tectonic Zone. Furthermore, dextral strike-slip faulting was recently documented also for the KFF, to the east of the KSF

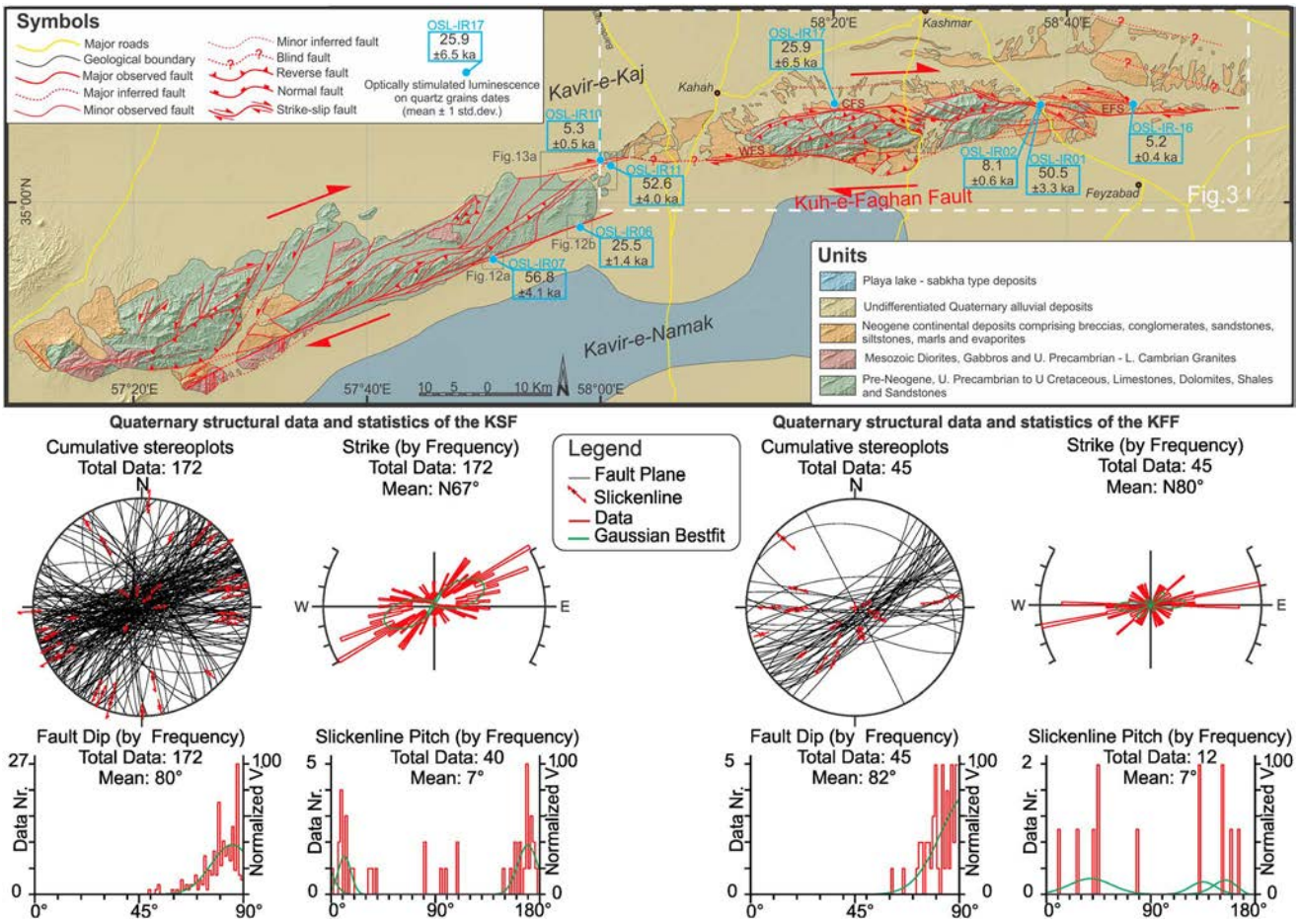

Figure 2. Simplified geological map of the KSF-KFF deformation zone along the northern edge of Lut Block (modified after *Nozaem et al.* [2013] and *Calzolari et al.* [2015]). Quaternary structural data are also shown. Fault population analysis was performed through the software Daisy 3 by *Salvini* [2004; http://host.uniroma3.it/progetti/fralab].

[*Calzolari et al.*, 2015] (Figures 1 and 2). The KSF and KFF are located ~40 km south of the subparallel, active sinistral DF [*Tchalenko et al.*, 1973; *Fattahi et al.*, 2007; *Farbod et al.*, 2011] (Figures 1 and 2). Remarkably, *Javadi et al.* [2013, 2015] documented a polyphase kinematic history for the DF, with a major kinematic reversal from dextral to sinistral slip during late Miocene-early Pliocene times.

2.1. Local Geology

The KSF-KFF system defines a ~150 km long, SW-NE to E-W striking, segmented linear topographic relief, with elevations up to ~1800 m above sea level (asl). It is surrounded by Quaternary alluvial deposits of the Kavir-e-Namak (southern) and Kavir-e-Kaj (northern) plains.

The seismicity of the KSF-KFF area (Figure 1b) is poorly known, although it has been discussed by *Berberian* [1976, 1977], who generally describes the KSF as a Quaternary fault. Some earthquake epicenters have been localized in the KSF area, with maximum recorded magnitude between 4 and 5 and focal depths less than 30 km. Several historical earthquake epicenters are located along the KFF, with maximum recorded magnitudes between 6 and 7 and inferred maximum focal depths between 35 and 70 km (Figure 1b). The few focal mechanism solutions available for northern Central Iran (Figure 1b) document strike-slip and reverse kinematics along the main fault systems. Nevertheless, their scarcity and contrasting kinematics suggest that they cannot be used reliably to infer the overall kinematics of the fault systems.

The axial zone of the KSF-KFF system is made up of Neoproterozic and Paleozoic-Mesozoic basement units [*Eftekhar-Nezhad et al.*, 1976; *Ruttner et al.*, 1970; *Sahandi et al.*, 2010; *Nozaem et al.*, 2013; *Rossetti et al.*, 2015] in fault contact with the Neogene (continental deposits comprising conglomerates, sandstones, siltstones, and evaporites) and Quaternary deposits of the Kavir plains (Figure 2).

The overall fault system architecture is controlled by spatially distributed dextral strike-slip tectonics. Field evidence documented that most of the fault displacement within the KSF-KFF system occurred in pre-Quaternary times, with major fault damage zones developed within the Neogene units [*Nozaem et al*., 2013; *Calzolari et al*., 2015]. Two major episodes of fault-related exhumation along the KFF, in the early Miocene (~18 Ma) and early Pliocene (~4 Ma), respectively, indicate that the KFF activity was punctuated, nucleated in the west and propagated eastward [*Calzolari et al*., 2015]. A source-to-sink scenario was reconstructed for the first faulting/exhumation episode based on the structural and depositional architecture of the Neogene deposits widely outcropping along the KFF. The second faulting episode, at ~4 Ma, caused the final fault zone exhumation and the current fault zone architecture.

Faulted Quaternary deposits in the KSF-KFF system have been previously documented by *Nozaem et al*. [2013] and *Calzolari et al*. [2015]. A total of 216 fault surfaces (51 with striated surfaces) were examined from the Quaternary deposits (Figure 2). The KSF shows the maximum frequency distribution of fault strikes at 61°N, with a subordinate population at 30°N. Faults show high angle to subvertical dips, with a maximum frequency of fault-strike distribution at 85° and a mean dip value of 80°. The frequency distribution of the pitch angle of the measured slickenlines attests to dominant strike-slip kinematics with a mean pitch value of 7°. A minor dip component of slip is documented in the slickenlines, coherent with a transpressive regime of shearing. The KFF shows a fault-strike distribution with a maximum at 87°N and high angle to subvertical dips, with a mean dip value of 82°. Despite the few measured slickenline pitch angles (11 data points), dominant dextral strike-slip to oblique-slip (transpressional) kinematics (pitch angle $< 45°$) are documented.

2.2. Geomorphological Background

In arid environments such as Central Iran, the processes allowing the formation of well-developed alluvial fans and fluvial terraces are (i) channel shifting favored by the lack of vegetation cover; (ii) occasional flash floods capable of revitalizing the streams and allowing them to evacuate large volumes of sediments; and (iii) production of large quantities of debris by weathering processes [*Bull*, 1977; *Cooke et al*., 1993; *Harvey*, 1997]. Pediments are also widespread in arid environments and can be generally considered as planation surfaces of regional extent, which develop mainly through sheetflood episodes during base-level stability [*Whitaker*, 1979; *Dohrenwend and Parsons*, 2009].

Erosion/deposition dynamics of alluvial systems are sensitive to tectonics, climate, or other locally acting factors (e.g., slope and area of the feeding catchment), along with the resulting hydrological parameters [e.g., *Schumm*, 1977; *Hancock and Anderson*, 2002; *Vandenberghe*, 2003; *Bookhagen and Strecker*, 2012]. Therefore, different conceptual models for alluvial landform development have been proposed so far [e.g., *Bridgland and Westaway*, 2008]. With respect to the major mountain chains of Iran, alluvial fan aggradation has been associated with Quaternary cold periods, such as described by *Beaumont* [1972] for the southern piedmont of the Alborz Mountains, and by *Dufaure et al*. [1978] for the Zendan fault area in southeast Iran. Recently, *Walker and Fattahi* [2011] reviewed the regional distribution and age of late Quaternary deposits of Central Eastern Iran. They recognized that several generations of alluvial fans, as well as a regional arrangement of fluvial terraces and playa lake deposits, could be explained by Late Pleistocene and Holocene environmental changes, with aggradation phases occurring between ~30 and 13 ka and between ~9 and 7 ka, alternating with erosive phases. They also provide suggestions, even if less well constrained, of alluvial fan abandonment at 40-60 ka. In situ produced cosmogenic ^{10}Be [*Regard et al*., 2006] provided surface abandonment ages for different Quaternary alluvial surfaces in the Hormoz Strait area at 5.6 ± 0.6 ka (end of the mid-Holocene humid period), 8.4 ± 1.0, 12.8 ± 1.0 ka (onset of the dry Younger Dryas cold and dry episode), and 20.1 ± 1.5 (end of the Last Glacial Maximum). Similar and coeval generations of alluvial fans have been recognized along the Nayband Fault, on the western margin of Lut Block [*Foroutan et al*., 2014], and an infrared stimulated luminescence (IRSL) age of ~10 ka was obtained for the deposition of the Shesh-Taraz fan along the DF [*Fattahi et al*., 2007].

The above results from Central Iran are mostly in agreement with a climate-forcing model in which the alluvial surface abandonment occurs mainly at the end of wet periods. In this model higher rainfall leads to higher erosion rates in ranges and increased deposition at their foot; in contrast, lower rainfall leads to reduced sediment flux and incision at the piedmont of the ranges. While aggradation seems to be clearly correlated to regional wet climatic phases, some abandonment ages are not regionally correlated and have been associated with localized enhanced tectonic activity without regional impact [*Regard et al*., 2006]. In fact,

the Quaternary morphoevolution is likely controlled also by the erosion/deposition dynamics of the drainage network developed on single fault-controlled ridges.

Quaternary faults locally displace linear (stream channels) and areal (alluvial fans and fluvial terraces) geomorphic markers, as widely documented for the narrow deformation belts bounding the CEIM [*Walker and Jackson*, 2004; *Allen et al*., 2004, 2011; *Farbod et al*., 2011; *Foroutan et al*., 2014]. Nonetheless, such displacements are evident only if very localized fault strands cut through the landforms, such as in the case of the DF [*Tchalenko et al*., 1973; *Fattahi et al*., 2007; *Farbod et al*., 2011; *Javadi et al*., 2013]. In other cases, especially where alluvial fans apexes are located on the margin of fault-bounded mountain front, these geomorphic markers do not show substantial offsets, even if Quaternary faulted deposits are documented at the outcrop scale [*Nozaem et al*., 2013].

In the KSF-KFF area, Quaternary alluvial fans and terraced fluvial deposits lie upon angular and erosional unconformities that cut across the strongly tilted Neogene units. In the KSF area, three generations of alluvial fans, locally in telescopic arrangement, have been described by *Nozaem et al*. [2013]. Despite the lack of direct dates, they used surface roughness as a diagnostic characteristic for correlating the KSF alluvial fans to three generations regionally recognized and described by *Walker and Fattahi* [2011]. However, the architecture, age, and the tectonic deformation of such planar geomorphic markers are still unknown, especially around the KFF system.

3. Materials and Methods

The incision and deformation of pediments, as well as the architecture of alluvial fans and fluvial terraces, can in some cases provide unambiguous evidence of tectonic activity, especially uplift, which raises abandoned surfaces to progressively higher elevations [*Bridgland*, 2000; *Maddy et al*., 2001; *Westaway et al*., 2004; *Wegmann and Pazzaglia*, 2009; *Schildgen et al*., 2012; *Yildirim et al*., 2013]. In such cases, geomorphological survey combined with geochronological methods can constrain deformation rates along specific structures [*Strecker et al*., 1989; *Lavé and Avouac*, 2001; *Pérez-Peña et al*., 2009a; *Wilson et al*., 2009; *Yildirim et al*., 2013].

We performed topographic analyses of the KFF to detect the influence of the inherited topographic signal, associated with the long-term fault history, on the Quaternary morphoevolution. A digital elevation model (DEM) of the study area with a 10×10 m cell size was produced using data from topographic vector maps from the National Cartographic Center of Iran. Topographic contours, independent elevation points, and river network data were interpolated using the ANUDEM algorithm 5.3 [*Hutchinson et al*., 2011]. We first produced slope angle, aspect, and local relief maps. The latter were obtained by calculating the residual between the maximum and minimum elevations averaged within a circular moving window with a radius of 300 m, corresponding to the average main valley spacing [*Scotti et al*., 2013, and references therein]. Then we performed a topographic analysis [*D'Agostino and McKenzie*, 1999; *Molin et al*., 2004; *Wegmann et al*., 2007; *Molin et al*., 2012] of the KFF ridge by means of (i) filtered topography at the local scale (using Focal Statistics Tool of ArcGIS 10.1 for calculating the average elevation in 1, 2.5, 5, 10, and 20 km radius circle areas), to assess the spatial distribution of topographic signals of the KFF at different wavelengths; and (ii) five across- and along-ridge swath profiles [*Mitchell and Montgomery*, 2006; *Telbisz et al*., 2013; *Hergarten et al*., 2014] to illustrate the ridge-scale distribution of minimum (base level), mean, and maximum (crest envelope) elevations and, implicitly, of local relief as a proxy of uplift-driven river incision.

We mapped the Quaternary alluvial landforms and deposits associated to the fault-related ridge of the KFF, by integrating geomorphological field surveys with DEM terrain analysis and aerial photo interpretation. Then we dated such deposits with OSL techniques to (i) correlate the mapped Quaternary deposits to the ones already dated in the region; (ii) use these landforms as geomorphic strain markers; and (iii) provide a minimum age constraint to the Quaternary faulting along the northern edge of Lut Block. Samples were collected from key stratigraphic horizons and from the Quaternary faulted deposits along the KFF. In particular, we concentrated sampling on the faulted alluvial deposits, possibly from all the recognized generations. For a wider correlation, we present here also the OSL ages obtained for the samples collected in correspondence to the faulted alluvial fan generations of the KSF described by *Nozaem et al*. [2013] (see Figure 2 for location).

The quartz grains used for OSL dating originally come from the pre-Neogene bedrock. For each site, we sampled at a depth >1 m below the top depositional surface or erosional surfaces within the deposit to avoid

the risk of rejuvenated ages. The OSL data where acquired at the LABER OSL Lab, Waterville, Ohio (U.S.). Details on the analytical methods and protocols are provided in the supporting information files.

Successively, we analyzed the dated Quaternary alluvial fans and fluvial terraces as passive geomorphic strain markers to constrain surface deformation associated with Late Quaternary faulting. To assess if any fault-related uplift tilted the Quaternary deposits in the KFF system, ideally one would reconstruct the original bottom and top surfaces of the deposits, essentially using them as geomorphic markers. This is not an easy task, as in most cases such surfaces are not exposed and/or have been incised and reshaped by erosion. Nevertheless, the northern flank of the western sector of the KFF ridge provided a good area to test for fault-related tilting during the Quaternary. We performed a statistical analysis of alluvial fan slope angle focused on two areas where the fan systems are approximately oriented N-S. For the analysis we used a purposely developed routine to extract, from the DEM of the area, the elevation data points of the top surface remnants of single alluvial fan, excluding the areas of the fans that have been reincised by stream channels (see supporting information files for methodological details and complete numerical results). The advantage of performing a statistical analysis of the alluvial fan slope angle is that it can provide averaged slope values over a population of fans (for each generation and within different sectors). Thus, differences among the obtained averaged values that are higher than the associated slope estimation error can be considered as indicative of regional controlling factors and independent from locally variable factors influencing the slope of each single alluvial fan, such as source area, water discharge, and sediment supply [*Whipple and Trayler*, 1996; *Whipple et al*., 1998]. The statistical significance of the slope angle analysis is discussed in the supporting information files.

Finally, to assess any fault-related uplift in the eastern sector of the KFF ridge, we analyzed the longitudinal (N-S) variability of height and thickness of different generations of fill terraces, along one of the main rivers cutting different fault segments.

4. Topography of the KFF

The KFF defines an E-W oriented, up to 17 km wide, linear ridge reaching a maximum elevation of ~1700 m asl and dropping in elevation out to the east. The KFF-associated ridge can be subdivided into two main topographic domains (Figure 3a). The ~42 km long western domain is prominently elevated above the southern Kavir-e-Namak salt plain. It exhibits an axial region characterized by rugged and steep terrain (slope angle $>15°$; Figure 3b) and high local relief (>100 m; Figure 3c). The peripheral areas are defined by less elevated and gentler sloping terrain (slope angle ~2–5°) with lower local relief (<50 m) (Figure 3c) generally corresponding to bajadas of Quaternary alluvial fans. The boundaries between axial and peripheral areas of such domains are marked by sharp slope breaks located in correspondence of the fan apexes (Figure 3b). The latter are located close to the main fault strands bounding the deformation zone, hereafter named the western fault strand (WFS), the central fault strand (CFS), and eastern fault strand (EFS) (Figures 2 and 3a). Narrow linear ridges characterize the topography along most of the fault segments, thus suggesting that localized bulging is associated with fault displacement. This is particularly evident for the western tip of WFS, the CFS, and the fault segments to the south of the EFS.

The linear topography of the KFF is internally interrupted by low relief areas, both within the western and eastern topographic domains and at their boundaries. Such low relief areas developed where the main dextral fault strands bend southeastward. In particular, the low relief area that interrupts the linear topography of the western topographic domain matches the lozenge-shaped transtensional basin described by *Calzolari et al*. [2015], which was generated by the four main fault segments of the southeastward bending termination of the CFS and filled by Neogene deposits (Figure 2). The ~23 km long eastern domain is bounded to the south by the EFS and shows an overall eastward narrowing and decrease in elevation and relief (Figure 3). It is dissected by a southward draining river channel, which separates two subdomains with different topographic characteristics. To the west, a broadly E-W elongated, oval-shaped area of high relief, ~10 km long and 3.5 km wide, shows discontinuous E-W oriented narrow ridges and associated valleys. To the east, a very narrow ~10 km long, E-W oriented linear ridge marks the eastern tip of the KFF. The whole KFF ridge shows a prominent, roughly E-W oriented drainage divide that separates a broader and gentler northward draining slope from a narrower and steeper southward draining slope (Figure 3d).

The local-scale topographic filtering quantifies the wavelength of the above described topographic domains (Figure 4), which mirror the eastward increase in shear localization within the main fault zones. The 20 km filter

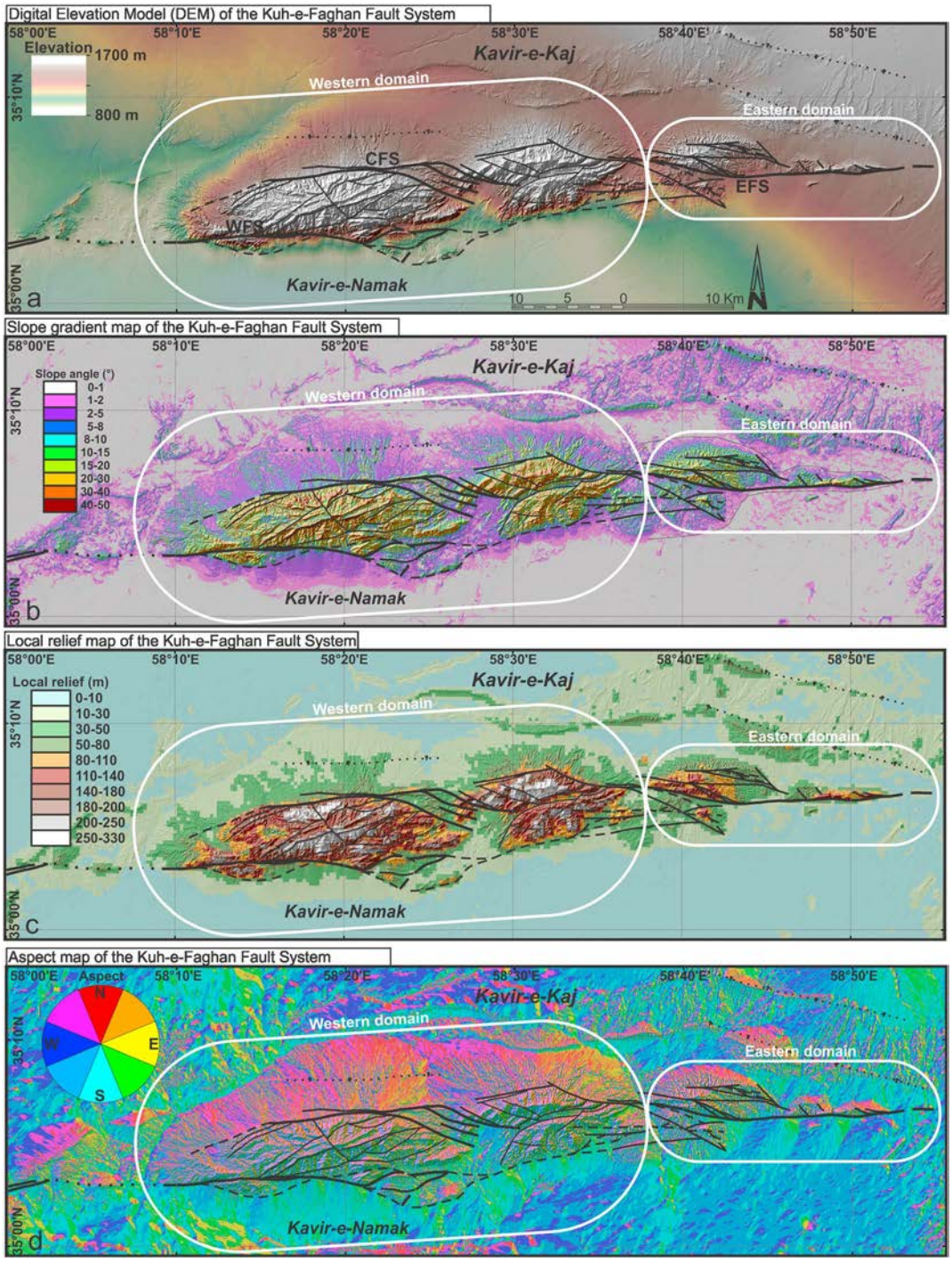

Figure 3. Maps of the study area extracted from a 10 × 10 m digital elevation model, with faults marked in black. (a) Topography by DEM. (b) Slope gradient map. (c) Local relief map. (d) Aspect map.

outlines a gently southwestward dipping regional surface that likely represents the background topography, averaging the height drop between Kavir-e-Kaj and Kavir-e-Namak plains. The western topographic domain starts to be resolved with the 10 km filter and the eastern topographic domain with the 2.5 km wavelength.

This analysis is confirmed by the topographic data of the longitudinal swath profile (SWP5 in Figure 5), which outlines the above described, fault-bounded longitudinal topographic domains. The western topographic domain shows higher maximum topography and relief, with a relatively constant local base level

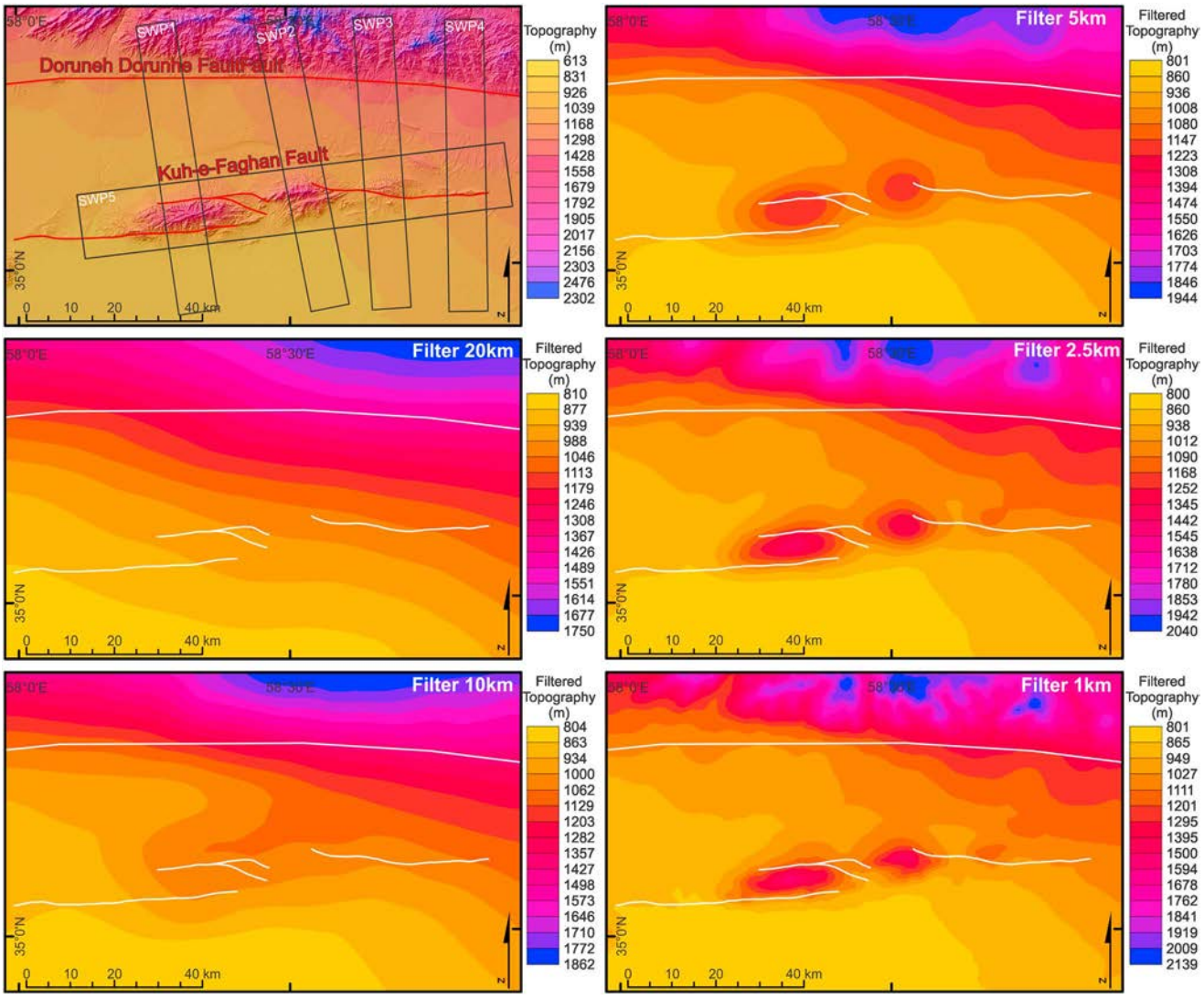

Figure 4. Filtered topography analysis performed on a 10 × 10 m (cell size) digital elevation model. Progressively smaller (from 20 to 1 km) radial filter was implemented.

(minimum topography). The eastern topographic domain is characterized by an overall eastward decrease of the maximum topography concurrent with an increase of the minimum topography of the range. The eastward increase of minimum topography corresponds to a progressively higher local base level of erosion. The four across-strike-oriented swath profiles outline the local topographic signal of the KFF fault strands and DF, marked by sharp breaks in local relief and/or by very narrow fault-related ridges (Figure 5). Finally, in the western part of the KFF, the southern flank is steeper, narrower, and with higher relief than the northern one. Finally, the northern base level of the ridge is a well-developed flattish plain, up to 170 m higher than the southern plain (Figure 5). These plains are bordered by low-gradient alluvial fan systems, which connect them to the slopes of both the DF-related ridge and the KFF western topographic domain. Such plains progressively disappear eastward, where the more elevated erosional unconformity sculpted into the Neogene units is partly covered by a southward dipping bajada of alluvial fans, fed only by the DF-related ridge.

5. Geomorphic Signal of the KFF

5.1. Evidence of Drainage Network Evolution

The KFF area is far from the sea and dominated by the growth of fault-related linear ridges separated by intermontane basins. In such a landscape, it is likely that drainage system rearrangement occurred during

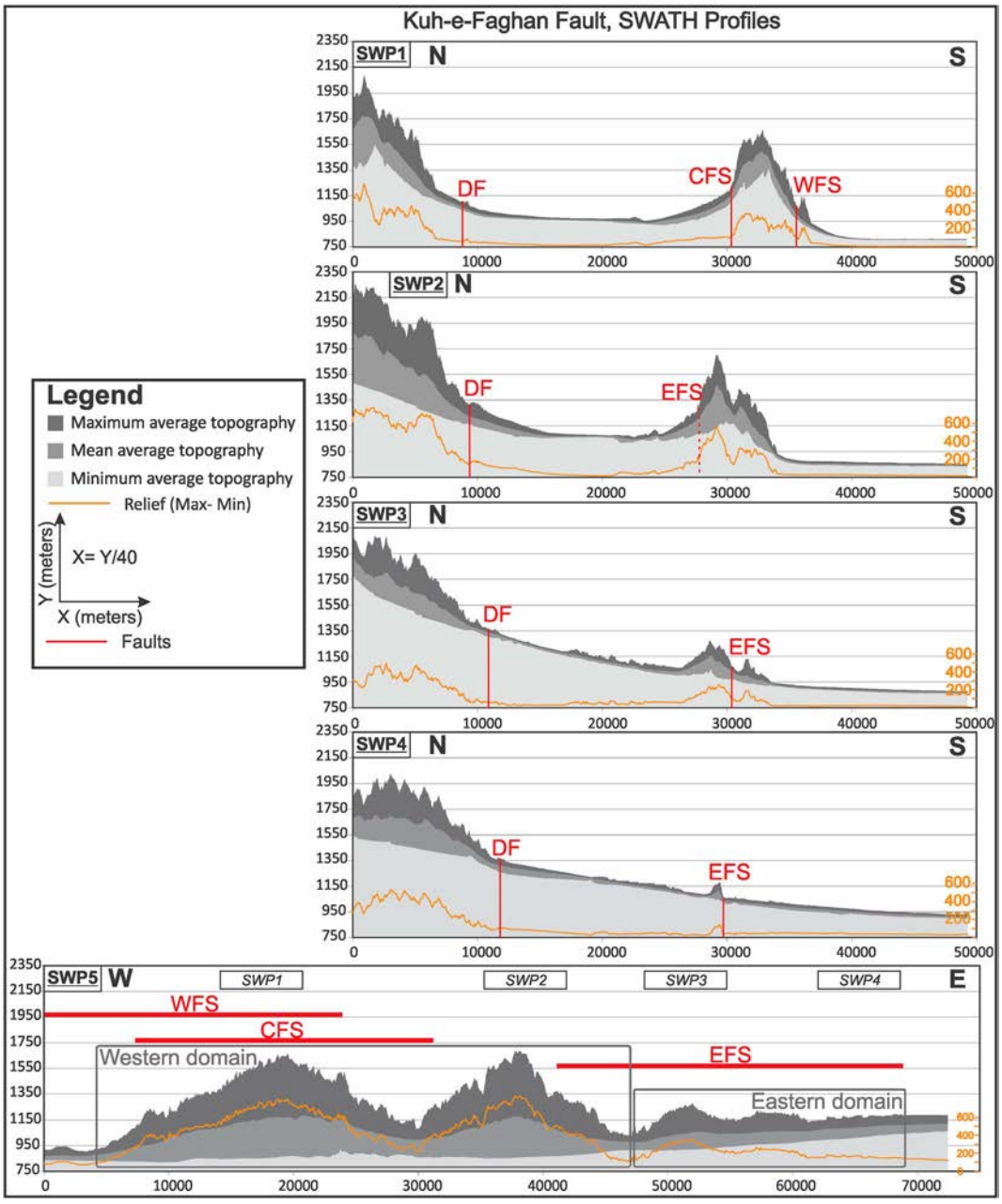

Figure 5. Swath profiles (40 times vertical exaggeration) across strike of the KFF (SWP1 to SWP4) and along strike of the KFF (SWP5) extracted from a 10 × 10 m digital elevation model. Locations of the swaths are shown in Figure 4.

the Quaternary, most likely controlled by changes in local base level [*Jackson et al.*, 1996; *Bennett et al.*, 2006]. Local base levels are represented by the Kavir-e-Namak (southern) and Kavir-e-Kaj (northern) plains. They exhibit a maximum height drop of ~170 m in the west, which progressively wanes eastward. Presently, the northern plain is drained by two main competing rivers that in their middle reaches cut into the ridge (Figure 6). These rivers mark the lateral boundaries of the western topographic domain of the KFF ridge. Their upper reaches are westward and eastward flowing, respectively, with a very low divide, clearly closer to the eastern boundary of the topographic domain. The latter evidence suggests that the westward flowing river exerted the most effective headward erosion. The headward erosion of the western river caused the northern plain to be captured by the southern one, where their difference in elevation is maximum (~170 m). This is suggested by the following geomorphic evidence (Figure 6): (i) the stream channels on

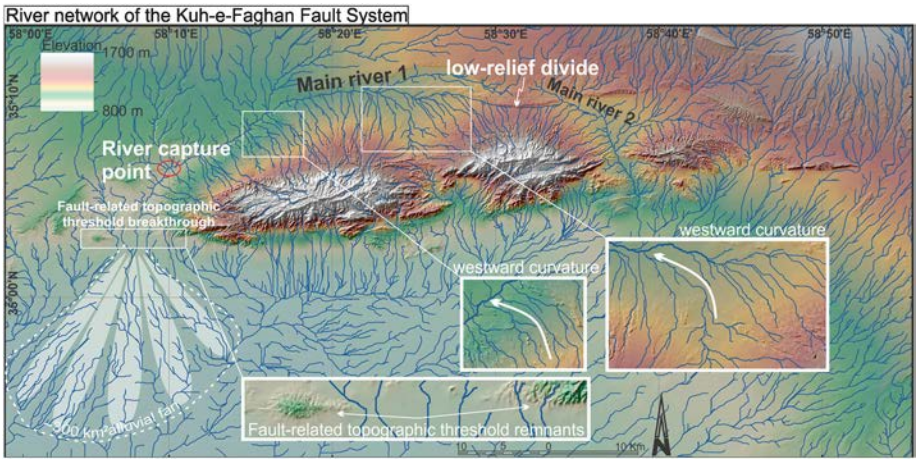

Figure 6. River network on DEM of the KFF area. Geomorphic evidences of drainage evolution are outlined.

the northern slope of the KFF ridge show a progressive westward curvature close to the confluence with the main westward flowing channel, which is typical of a progressively captured drainage system [e.g., *Pérez-Peña et al*., 2009b]; (ii) the height drop between the northern and southern plain shows a progressive eastward decrease, which conceivably gave higher stream power to the westward flowing river; and (iii) the latter

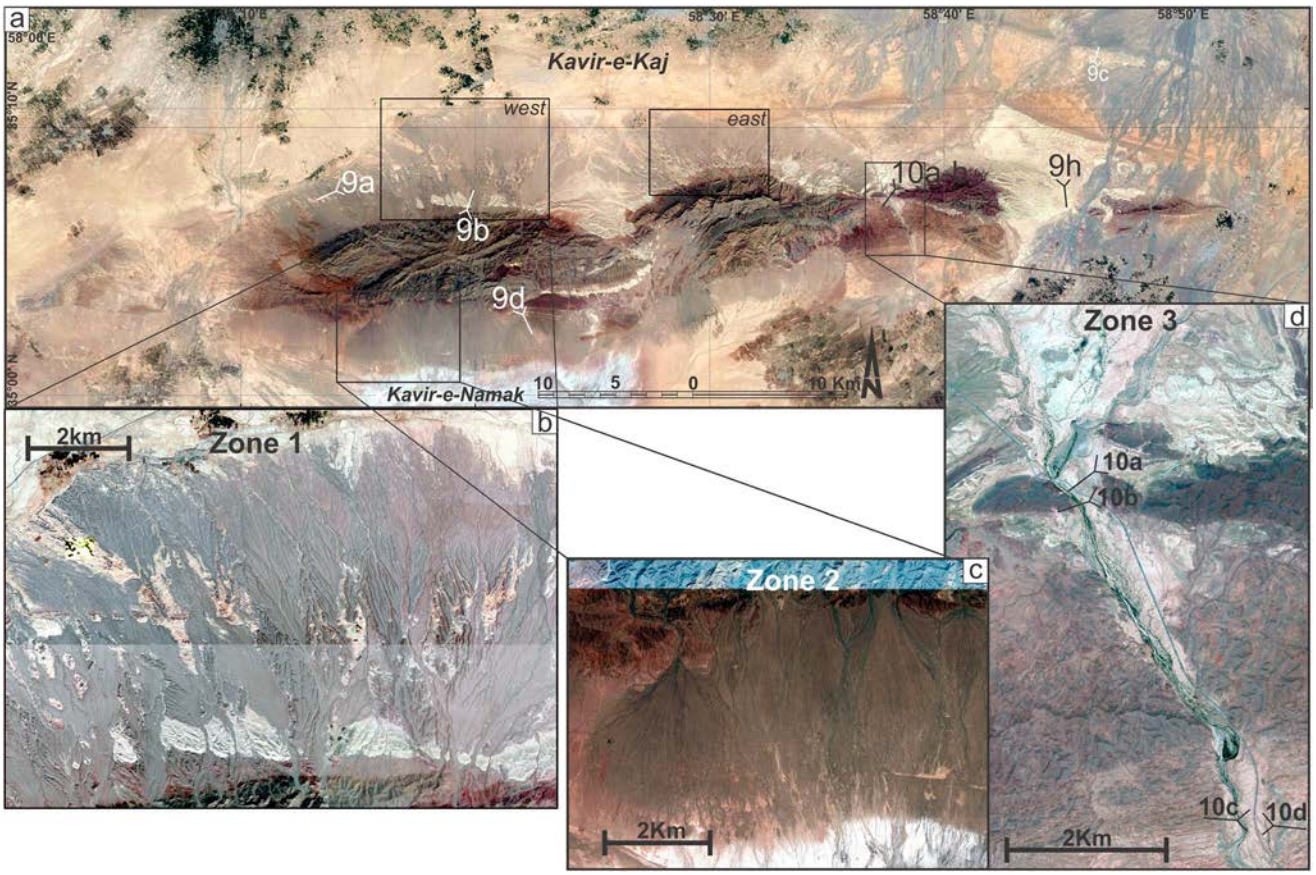

Figure 7. (a) Satellite image of the KFF area. The squares marked "west" and "east" indicate the areas where morphometric alluvial fan slope angle analysis was performed. (b) Blowup of the northwestern telescopically arranged Quaternary alluvial fan deposits (Zone 1). (c) Blowup detailing the southern stacked Quaternary alluvial fan deposits (Zone 2). (d) Blowup detailing the different generations of Quaternary terraced alluvial plain deposits (Zone 3). See Figure 8 for details on the distribution of the different Quaternary alluvial deposits.

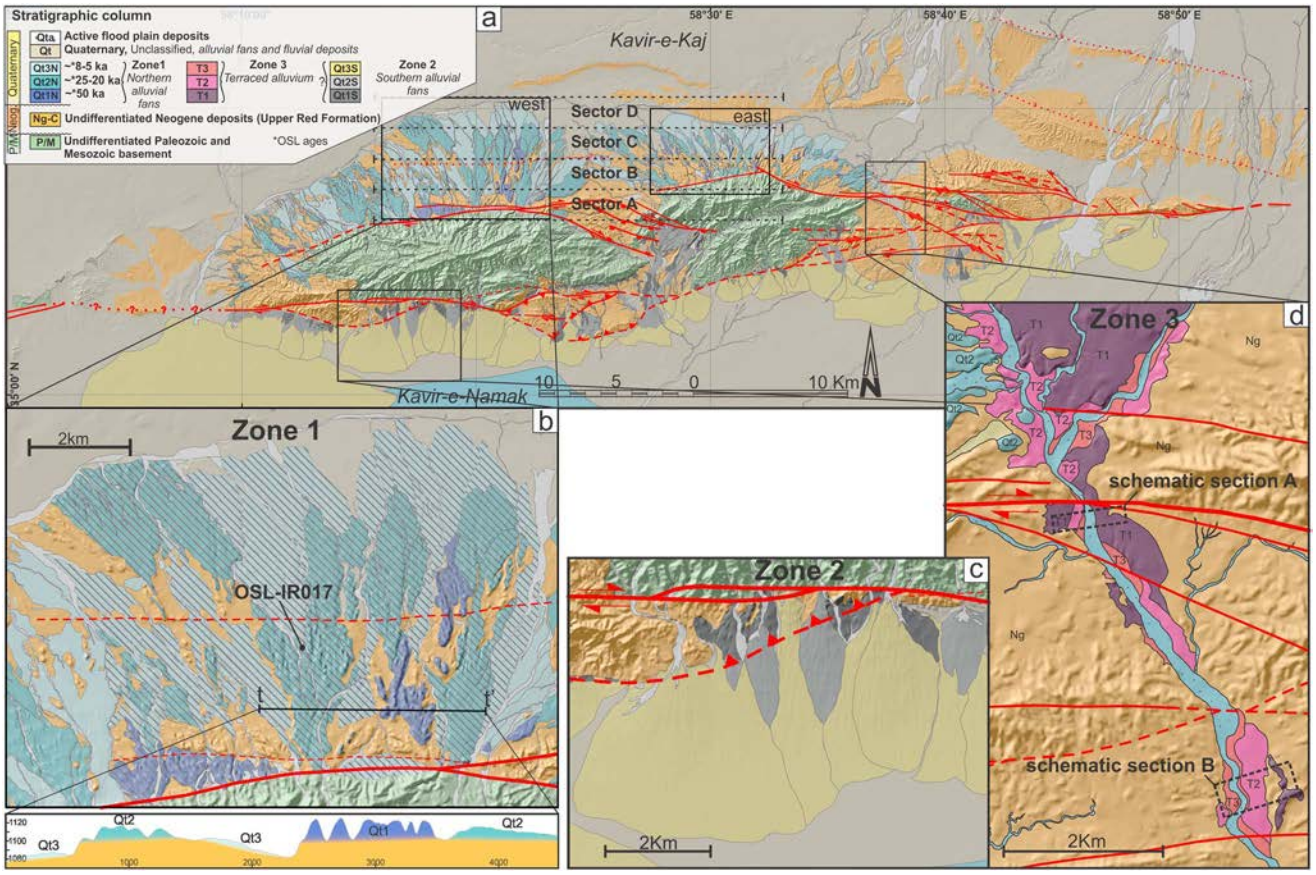

Figure 8. (a) Map of the KFF area showing the distribution of Quaternary alluvial deposits. The squares marked "west" and "east" indicate the areas where morphometric alluvial fan slope angle analysis was performed. The black dotted lines represent the boundaries of sectors in which morphometric analysis and statistics where performed (see text). (b) Blowup of the northwestern Quaternary alluvial fan deposits (Zone 1) with topographic section t-t' across Qt1N, Qt2N, and Qt3N deposits. Black hatched areas mark the alluvial fans used for the morphometric analysis. (c) Blowup detailing the distribution of the southern stacked Quaternary alluvial fan deposits (Zone 2). (d) Blowup detailing the distribution of the different generations of Quaternary terraced alluvial plain deposits (Zone 3); location for the schematic sections in Figure 16 is also outlined.

created a huge (~300 km^2) alluvial fan in the Kavir-e-Namak plain (Figure 6). On both sides of the huge fan apex, the remnants of a very narrow linear ridge associated with the WFS have been recognized. Thus, the huge fan likely originated by the breakthrough of such a topographic threshold that separated the northern plain from the southern one. In contrast, the eastward draining channel crosses the ridge without creating a similarly large fan. Thus, this channel could have developed through river antecedence during the eastward growth of the fault-related ridge.

5.2. Quaternary Landforms and Deposits

We mapped three generations of Quaternary alluvial landforms and deposits within the KFF (Figures 7 and 8). They consist of alluvial fans and river fill terraces composed of conglomerates, gravels, and sands, exhibiting various degrees of consolidation. The clasts making up the deposits principally consist of yellow, grey, and black fossiliferous limestone, dolomite, sandstone, and shale, indicating that the deposits were sourced from the basement and Neogene units. In the terraced alluvial plain deposits, subordinate amounts of quartz pebbles and volcanoclastic sediments are also present. Because these lithotypes are exotic in the KFF area, they were probably sourced from the DF area and transported to the KFF by the southward draining alluvial systems.

The oldest Quaternary deposits cover the planar erosional unconformity that cuts the tilted Neogene deposits. This unconformity can be traced regionally both to the north (Figures 9a–9c) and south (Figure 9d) of the KFF mountainous ridge and is therefore inferred to represent a paleopediment, striking subparallel to and

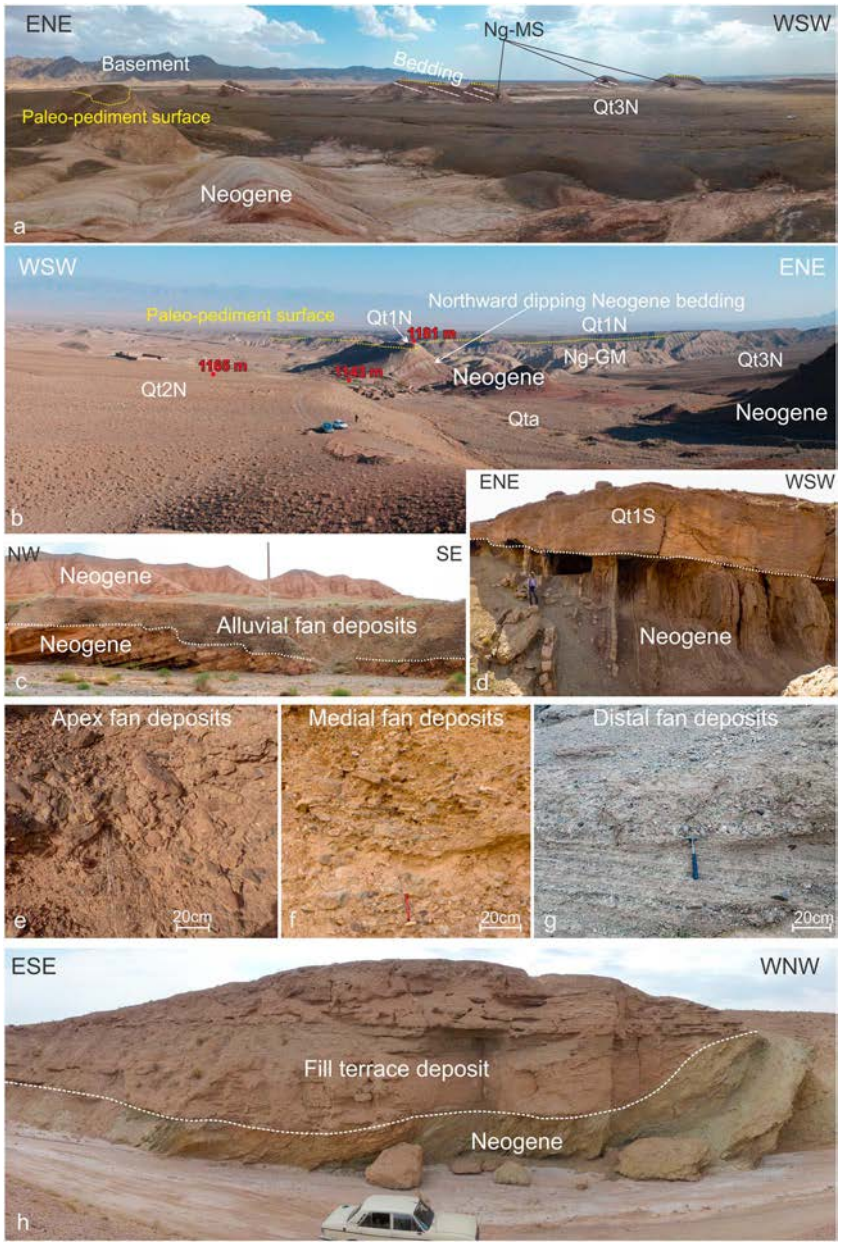

Figure 9. Outcrop examples of the Quaternary alluvial fan and alluvial plain deposits. Panoramic views of the alluvial fan deposits and their stratigraphic relations with the Neogene deposits in the geomorphological Zone 1 (see Figure 7 and text), viewed (a) from the northern alluvial plain toward the fault system and (b) from the fault system (the CFS) toward the alluvial plain. (c) Example of the Neogene-Quaternary erosional unconformity (paleopediment) tens of kilometers north of the fault system. (d) Example of the Neogene-Quaternary erosional unconformity (paleopediment) to the south of the KFF. Example of Quaternary fan deposits characteristics from (e) the fan apex zone to the fan (f) medial and (g) distal zones. (h) Outcrop example of the alluvial plain deposits in the geomorphological Zone 3. See Figure 7 for locations.

dipping away from the KFF prominent linear topography. It exhibits slope angles $<7°$, which tend to decrease away from the KFF structure.

The alluvial fans exhibit variable characteristics from the apex to the distal part. Chaotic, clast-supported, highly angular, proximal breccia and conglomerate deposits characterize the apex area (the first 200 to 300 m), with maximum particle size of 35 cm (Figure 9e). The central part of the fan system consists of relatively more texturally mature and rounded, matrix-supported conglomerates arranged into 30 to 100 cm thick beds, exhibiting normal grading and infrequent cross stratification in the upper part of the beds.

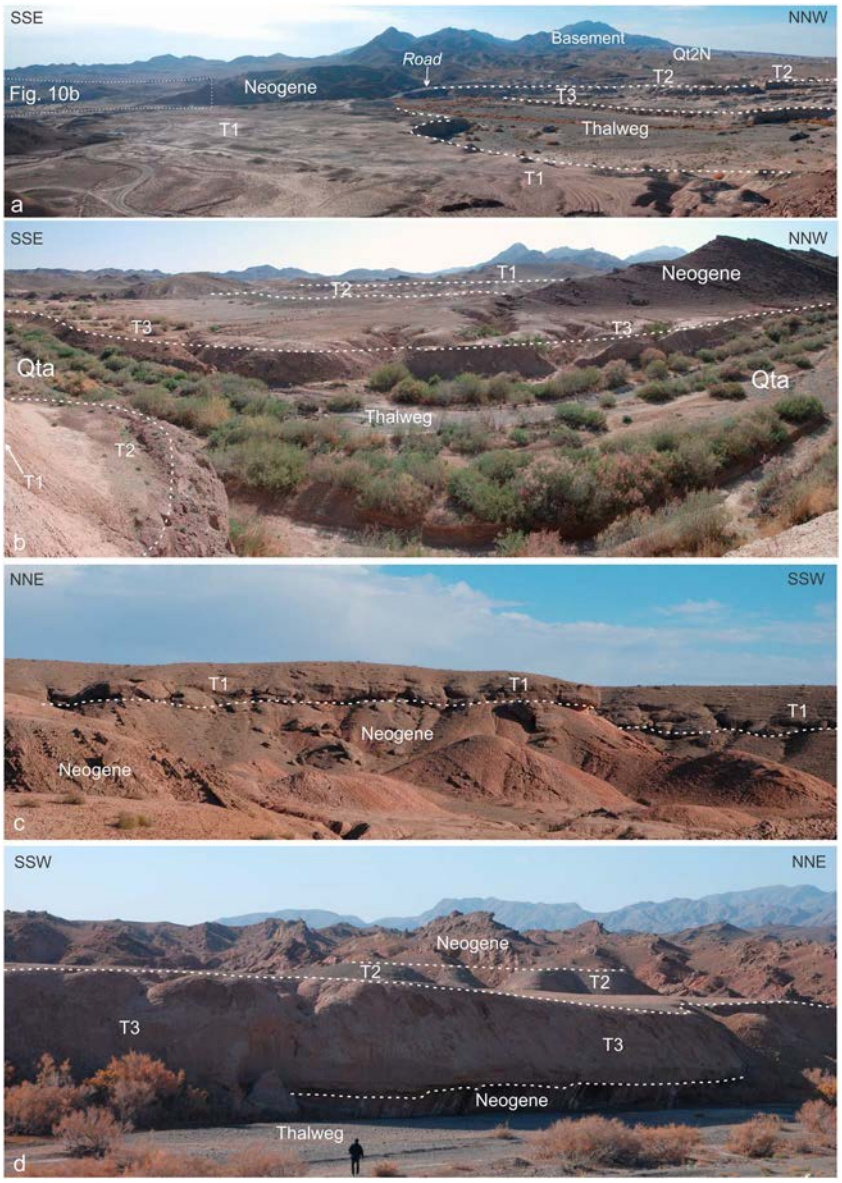

Figure 10. Panoramic view of the Quaternary fluvial terraces of Zone 3. (a) Height distribution of T1, T2, and T3 are shown close to the EFS, along with correlation with the alluvial fan deposits. (b) A detail of the topographic setting of T1, T2, and T3 is shown in the same area. Height distribution of T1, T2, and T3 are shown also in the vicinity of fault segments to the south of the EFS: (c) T1 terrace photographed from the top of T2; (d) T2 and T3 terraces. See Figure 8 for location.

In this area the clast size is up to 15 cm (Figure 9f). The distal portion of the fan deposits is characterized by cross-stratified and, at times, clinostratified gravelly sands, exhibiting normal grading and infrequent concave upward erosional surfaces. The deposits contain clasts with maximum particle size of 5 cm (Figure 9g). The terraced alluvial plain deposits principally consist of sandy, large-scale lenticular beds, exhibiting some cross stratification and concave upward erosional surfaces, with gravelly horizons (Figure 9h).

Based on the landform- and deposit-type associations, we recognized three major geomorphological zones in the KFF area. *Zone 1* is n the northern slope of the KFF western topographic domain, and it is cut by the CFS (Figure 8). *Zone 2* is south of the KFF western topographic domain, and it is cut by the WFS (Figure 8). *Zone 3* develops across the EFS and the other fault segments to the south (Figure 8), some of which are characterized by very narrow (<1 km wide) fault-related topographic ridges.

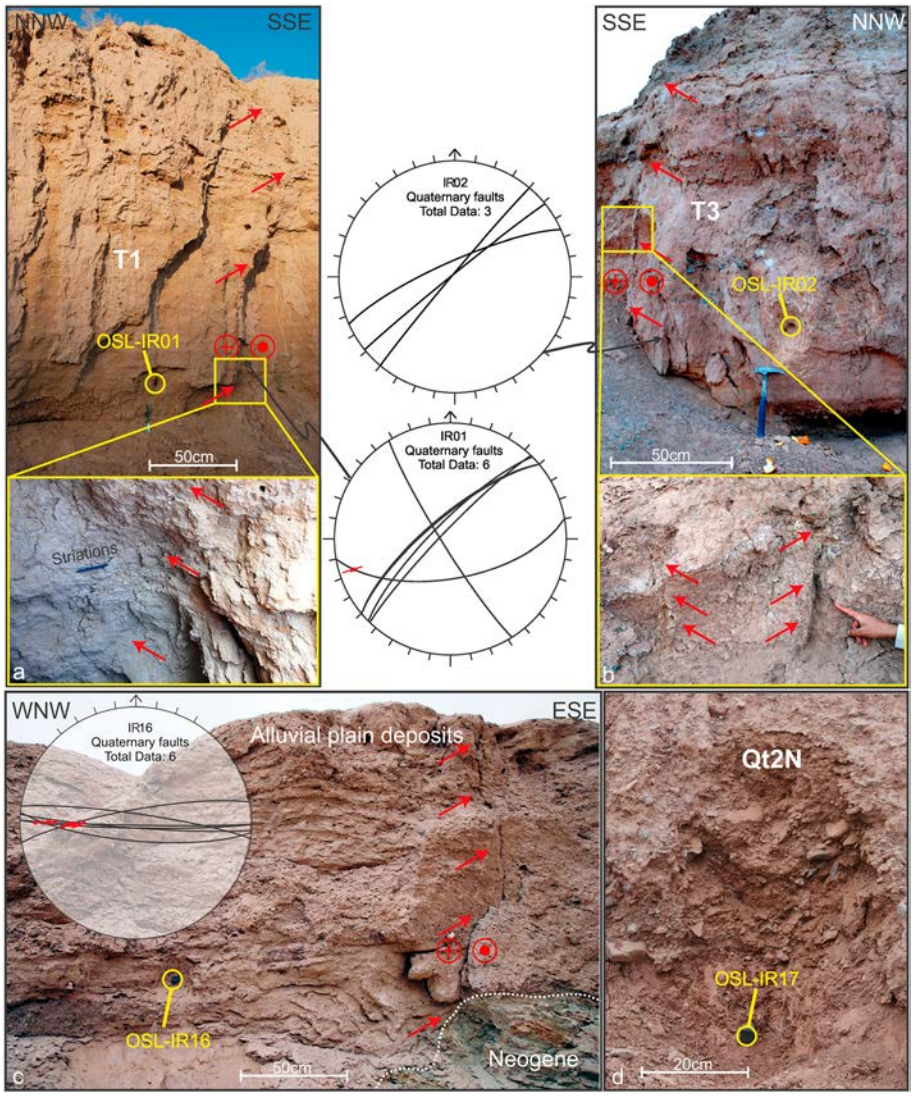

Figure 11. Quaternary faulting and OSL sampling sites along the KFF. See Figure 2 for sampling site location. (a) Detail of the sampling site in the faulted T1 fill terrace deposit; (b) detail of the sampling site in the faulted T3 fill terrace deposit; (c) detail of the sampling site in the faulted fill terrace deposit of the easternmost river dissecting the KFF ridge; (d) detail of the sampling site in the terraced Qt2N alluvial fan in Zone 1, close to the CFS of the KFF. Stereoplots of structural data are also reported for all the sites (stereoplot legend in Figure 2). Fault population analysis was performed through the software Daisy 3 [*Salvini*, 2004; http://host.uniroma3.it/progetti/fralab].

In *Zone 1* three generations of alluvial fans were identified (Qt1N, Qt2N, and Qt3N, Figure 8a). They can be distinguished by their degree of surface reincision (Figure 7b) and their relative top and bottom surface elevation, which systematically decreases from Qt1N to Qt3N (e.g., cross-section t-t', Figure 8b). In particular, the Qt1N alluvial fan deposits are generally poorly preserved and their fan geometry is often fragmented. They are always found lying above the paleopediment (Figures 9a and 9b), and their top surface exhibits extremely incised and rugged topography (Figure 7b). The plan shape of Qt2N alluvial fan deposits is better preserved and they exhibit relatively less incised top surfaces. They are entrenched in Qt1N, and often into their basal erosional surface (Figure 9b), with their bottom and top surface generally located at lower elevation than the Qt1N's. The Qt3N alluvial fan geometries are the best preserved and exhibit very little top surface incision. They are relatively deeply entrenched into both Qt1N and Qt2N fans, and they lie further below the regional erosional surface (Figure 9b). Collectively, the three fan generations display geometric relations and characteristics typical of telescopically arranged fan systems, with the youngest ones entrenched in the older ones, due to a progressive downslope shift of the fan apex. Nevertheless, in the distal

Table 1. OSL Dating Results

Sample	Deposit	Location		Elevation	K	U	Rb	Th	Moisture	Depth	Dose Rate	E.Dose	Age	Error
		Latitude (°N)	Longitude (°E)	(m)	(%)	(ppm)	(ppm)	(ppm)	(%)	(m)	(Gy/Kyr)	Gy (±1 σs)	(Kyr)	(s1)
IR16	T3/KFF_East	35.121461°	58.755644°	1040	1.45	1.7	57.9	6	10 ± 5	4	2.13 ± 0.12	10.99 ± 0.54	5.16	0.41
IR10	Qt3/KFF-KSF_West	35.048642°	57.994108°	875	1.43	2.1	53.8	6.1	10 ± 5	1.5	2.25 ± 0.12	11.89 ± 0.55	5.28	0.53
IR02	T3/KFF_East	35.115917°	58.625378°	971	1.7	0.26	60.2	6.82	10 ± 5	2.5	2.104 ± 0.132	16.97 ± 0.48	8.06	0.60
IR06	Qt2/KSF	34.973583°	57.969694°	850	1.05	0.11	48.2	2.08	10 ± 5	2	1.23 ± 0.10	30.58 ± 0.41	25.54	1.43
IR17	Qt2N/KFF_West	35.129372°	58.332183°	1050	2.01	2.3	108.5	10.7	10 ± 5	6	3.02 ± 0.17	78.09 ± 19.08	25.86[a]	6.50
IR01	T1/KFF_East	35.116389°	58.625794°	983	1.67	0.25	55.3	6.21	10 ± 5	4	2.059 ± 0.129	103.95 ± 5.31	50.49	3.34
IR11	Qt1/KFF-KSF_West	35.037828°	58.016147°	858	1.25	1.7	46.4	4.7	10 ± 5	1.5	1.92 ± 0.11	100.90 ± 4.59	52.59	4.04
IR07	Qt1/KSF	34.936777°	57.847815°	900	1.87	0.02	45.7	7.1	10 ± 5	2	2.231 ± 0.143	126.75 ± 1.92	56.82	4.10

[a]Low signal, may not be reliable age.

portion, they form a wide bajada that drains northward into alluvial plains that are in turn drained by the two above mentioned competing river systems flowing to the west and east, respectively.

In *Zone 2* three other generations of alluvial fans are documented (Qt1S, Qt2S, and Qt3S, Figure 8a). They form a wide bajada, which drains southward into the Kavir-e-Namak plain. Qt1S and Qt2S deposits are restricted to proximal regions of the bajada, close to the southern mountain front. They represent remnants of alluvial fan apexes, which are now suspended tens of meters above the present rivers draining the plain. Qt3S alluvial fans make up most of the southern bajada and extend from the mountain front to the southern plain. Collectively, the three fan generations of *Zone 2* exhibit a staked architecture, since the younger ones generally developed over the older ones, without a downslope shift of the apex (Figure 7c).

Zone 3 is characterized by three generations of fill terraces. These alluvial deposits were sourced both from the KFF topographically prominent linear ridge and the DF area (to the north) as attested by the presence of a mixed clast population of KFF basement rocks and volcaniclastic, quartz rich clasts from the DF area. The three generations of fill terraces are well preserved along the N-S reach of the eastern main river (Figure 8d), where the terraces (T1, T2, and T3) are perched at different elevation above the thalweg (Figure 10). There, the T2 and Qt2N deposits seem to be morphologically correlated, plausibly indicating coeval deposition (Figure 10a).

5.3. OSL Dating

We collected four samples from the KFF area (IR01, IR02, IR16, and IR17; Figure 11). Sample IR01 (Figure 11a) is from a mostly sandy alluvial deposit with gravelly lenses. The top surface of the deposit lies at ~983 m asl and corresponds to the highest (T1) of the three fill terrace levels of *Zone 3* (Figure 10). Sample IR02 (Figure 11b) is from a sandy layer of an alluvial deposit entrenched in the previous one. The top surface of the deposit lies at ~971 m asl and corresponds to the lowest (T3) of the above mentioned fluvial terraces (Figure 8d). Both the samples were collected along the prominent E-W striking fault scarp that defines the geomorphic expression of the EFS, where T1 and T3 alluvial terraces are extensively affected by a set of subvertical fractures (Figures 11a and 11b). The obtained ages for these deposits are 50.49 ± 3.34 ka and 8.06 ± 0.60 ka, respectively (Table 1). Sample IR16 (Figure 11c) is from a sandy-gravelly alluvial deposit from the terraced alluvial plain of the easternmost river dissecting the KFF ridge. The top of the deposit is 5 m above the present river bed, lies at ~1040 m asl, and provided an OSL age of 5.16 ± 0.41 ka (Table 1). The deposit is affected by E-W oriented subvertical faults cutting through the gypsiferous Neogene units and into the Quaternary alluvial deposits. Calcite slickenlines and small-scale drag structures are coherent with dextral kinematics (stereoplot in Figure 11c). Finally, sample IR17 (Figure 11d) is from a silty- to sandy-matrix-supported

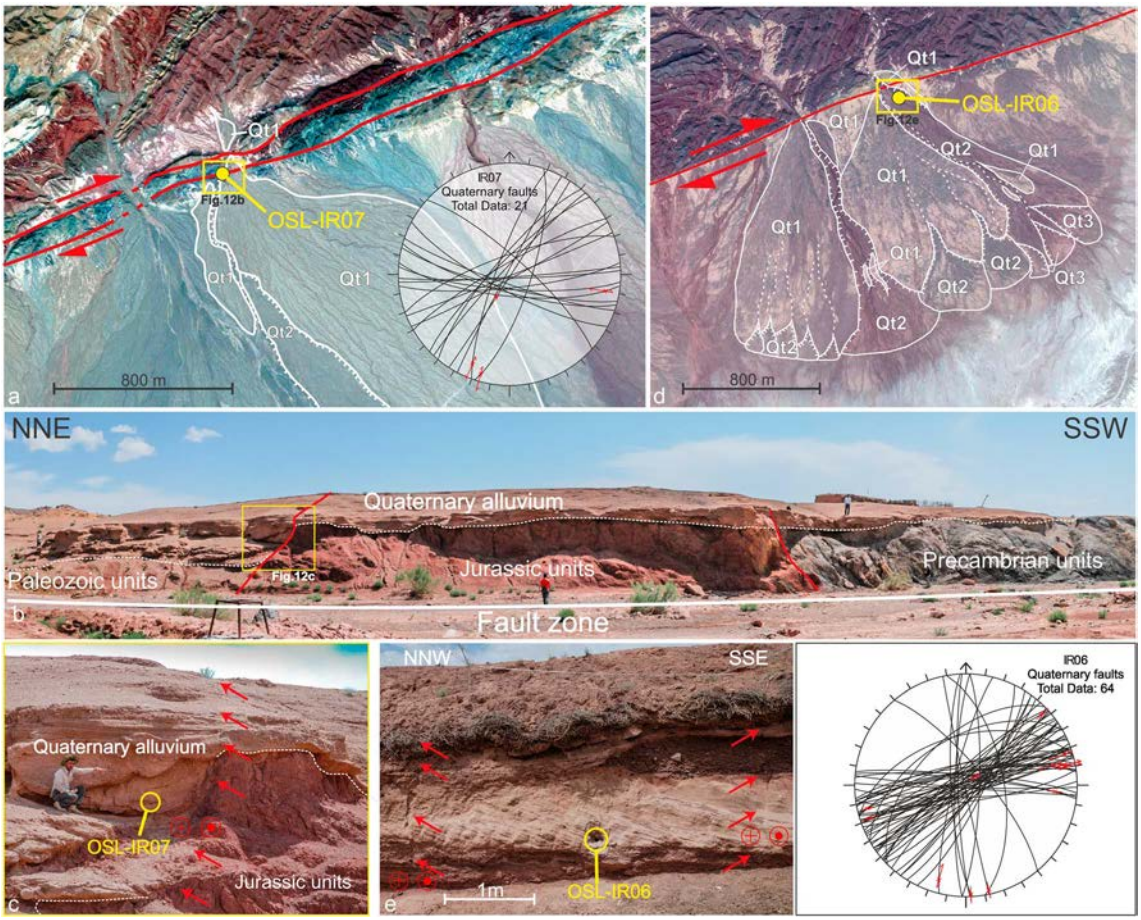

Figure 12. Quaternary faulting and OSL sampling sites along the KSF. (a) Satellite view of the Khakestary village site, with (b) a detail of the outcrop and (c) OSL sampling site. (d) Satellite view of the Kal-e-Sorkh village site, with (e) a detail of the outcrop and OSL sampling site. Stereoplots of structural data for the KSF sites are also reported for both the sites (stereoplot legend in Figure 2). Fault population analysis was performed through the software Daisy 3 [*Salvini*, 2004; http://host.uniroma3.it/progetti/fralab].

terraced alluvial fan deposit with gravelly lenses and belongs to the Qt2N alluvial fan generation in *Zone 1*, close to the CFS of the KFF (Figure 8b). The top surface of the deposit lies at ~1050 m asl, and obtained OSL age is 25.86 ± 6.50 ka (Table 1).

Additional four samples were collected along the KSF. In the Khakestary village (IR07 sampling site), the Quaternary alluvium, which unconformably overlies the Mesozoic and Paleozoic basement rocks, is cut by subvertical faults and associated fractures [*Nozaem et al*., 2013]. Faults are steeply dipping, striking from 20°N to E-W (stereoplot IR07 in Figure 12). The surface expression of the fault traces can be continuously followed on the ground (Figure 12a). Where interpretations were possible, kinematic indicators and stratigraphic offsets point to dominant dextral strike-slip kinematics with a minor reverse component. Sample IR07 was collected from a quite cemented sand layer of the older of two terraced alluvial fans, with alternating sand and gravel layers (Figure 12c). The top surface of the deposit lies at ~900 m asl, and the age provided by OSL dating is 56.82 ± 4.1 ka (Table 1). Close to the northeastern tip of the KSF at the Kal-e-Sorkh village (IR06 sampling site; Figure 12d), a number of faults and fractures cut Quaternary alluvial fan deposits [*Nozaem et al*., 2013]. The fault traces cut through the cross bedding in the alluvium, demonstrating an offset of a few centimeters. The main fault population strikes ENE. Where preserved, dextral strike-slip kinematics was reconstructed (Figure 12e and stereoplot on the right). Notably, several faults and fractures reach the surface, cutting the recent colluvium. Sample IR06 was collected from a terraced alluvial fan, with alternating sand and gravel layers. We sampled a medium sand level characterized by cross stratification. The top surface of the deposit lies at ~850 m asl, and the age provided by OSL dating is 25.54 ± 1.43 ka (Table 1).

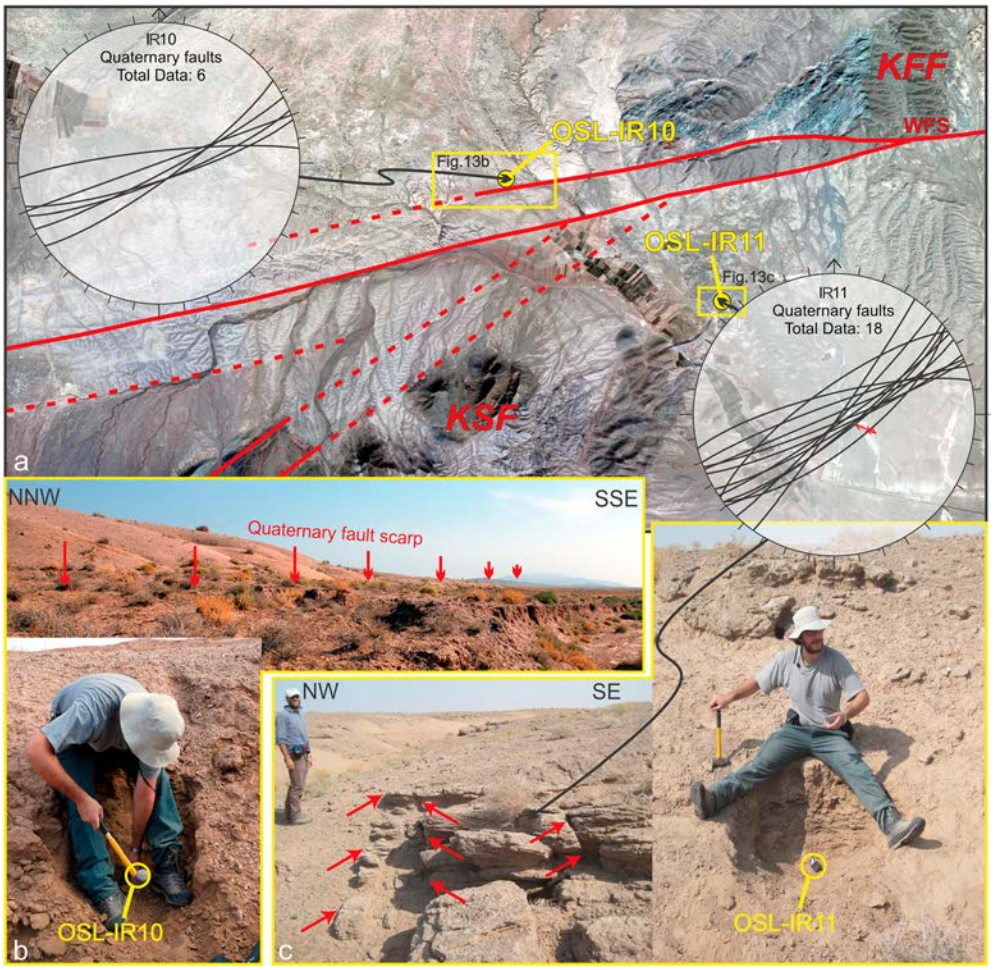

Figure 13. Quaternary faulting and OSL sampling sites in the area where KFF and KSF converge. (a) Satellite view of the area; (b) detail of the outcrop and OSL sampling site for sample IR10; (c) detail of the outcrop and OSL sampling site for sample IR11. Stereoplots of structural data are also reported for both the sites (stereoplot legend in Figure 2). Fault population analysis was performed through the software Daisy 3 [*Salvini*, 2004; http://host.uniroma3.it/progetti/fralab].

Two samples (IR10 and IR11) were collected from terraced and faulted alluvial deposits outcropping in the area where the KFF and the KSF converge (Figure 13a). Sample IR10 is from a silty-sandy terraced alluvial deposit affected by a fracture pattern coherent with the KFF deformation trend. The top surface of the deposit lies at ~875 m asl (stereoplot insert in Figure 13a). Sample IR11 is from a quite cemented silty-sandy terraced alluvial deposit with gravelly beds. The top surface of the deposit lies at ~858 m asl, and the deposit shows a E-W joint system that overprints a SW-NE one, each of them geometrically consistent with the deformation pattern characterizing the KFF and KSF, respectively (stereoplot in Figure 13c). The OSL age obtained from the deposit affected by the two sets of jointing (IR11 sampling site) is 52.59 ± 4.04 ka, while the age of the deposit affected by the lone E-W fracture pattern (IR10) is 5.28 ± 0.53 ka (Table 1).

OSL dating results are summarized in Table 1. Collectively, the ages of the Quaternary deposits surrounding the KSF-KFF system range from Late Pleistocene to the Holocene. Considering the ages obtained for river fill terraces and alluvial fans, coupled with the field evidence that Qt2N and T2 are coeval, we correlate the three generations of alluvial fans with the three levels of fill terrace deposits. Three age clusters for aggradation phases can be identified at ~6, ~25, and ~53 ka, respectively, which fit the regional ages obtained for Central Iran [*Walker and Fattahi*, 2011, and references therein]. Furthermore, the age of the younger faulted deposits (~5 ka) constrains the minimum age of dextral faulting along the KSF-KFF system to the Holocene.

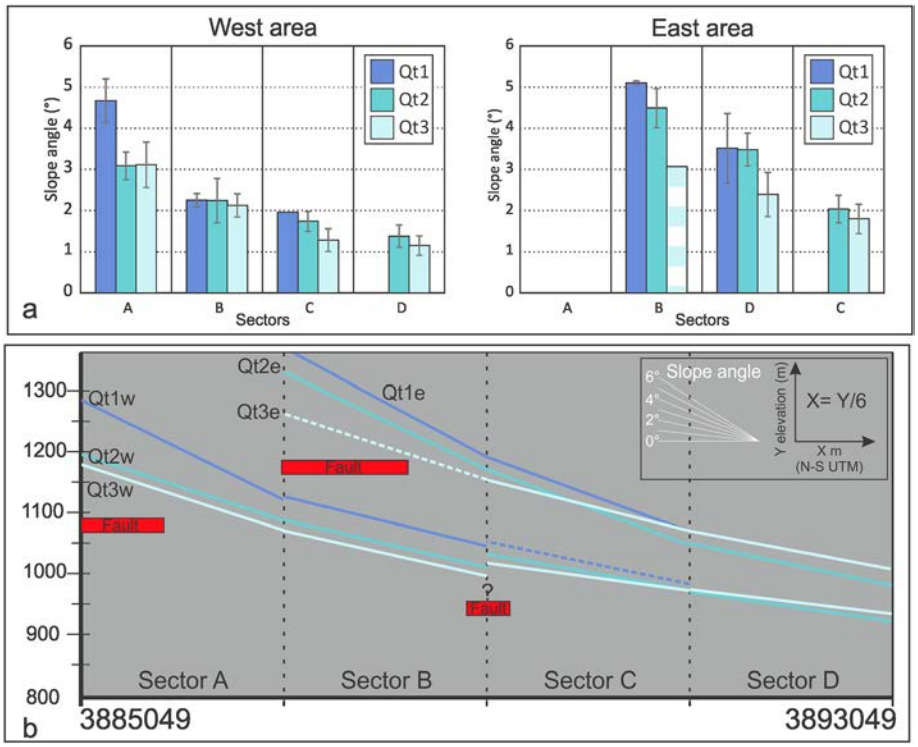

Figure 14. (a) Results of the statistical alluvial fan slope angle analysis for the four sectors (A, B, C and D in Figure 8a) and for areas "west" and "east" (see Figure 8 for location), with associated 1σ error bars. Qt3 bar in "east" area sector B is relative to a single fan and thus not statistically representative. (b) Mean alluvial fan slope angle and elevation have been also compared among the four sectors and for areas "west" and "east". The projected fault location extent is shown in red.

6. Fault-Related Localized Uplift Along the KFF

6.1. Alluvial Fans Along WFS and CFS

The geomorphic processes that create alluvial fans and pediments respond to base-level changes and tectonic activity along faulted mountain fronts [*Bull*, 2009]. In particular, in tectonically active regions, the arrangement of alluvial fan generations along a mountain front is the result of the competition among uplift rate, channel downcutting rate, and pediment aggradation/degradation. Typically, stacked generations of alluvial fans develop with dominant aggradation where uplift is the main base-level changing process. In contrast, telescopic alluvial fans develop if the apex of fan deposition shifts downslope, where stream channel downcutting is the dominant geomorphic process [*Bull*, 2007].

According to the alluvial fan architecture observed in geomorphological *Zone 1* (telescopic alluvial fans) and *Zone 2* (stacked alluvial fans), it seems that the northern front of the KFF ridge could have experienced more important stream channel downcutting than the southern one. This interpretation is in agreement with the drainage network evolution and in particular with the evidence that rivers draining the northern plain are deeply entrenched due to headward erosion that likely propagated from the western main river to the streams draining the northern slope (Figure 6). Conversely, *Zone 2* corresponds to the steeper and narrower limb (dip angle $>40°$) of the broad, E-W striking, asymmetric, and south verging antiformal fold, closer to the localized active deformation zone of the WFS and thus is likely to have experienced uplift-driven base-level changes (Figure 2). Because the alluvial fan sets in the two geomorphological zones are coeval, climate cannot be invoked as the factor controlling their architecture, although it likely controlled the timing of their aggradation. The dominant effects of channel downcutting versus uplift along the northern slope was most likely influenced by the drainage network rearrangement described in the previous sections. Nonetheless, even if drainage rearrangement along the CFS can be invoked as the main base-level changing process, eventual ongoing fault-related uplift could have been recorded by the alluvial fans and could be unequivocally recorded by progressive tilting of the alluvial fan surfaces [*Bull*, 1977; *Giano*, 2011].

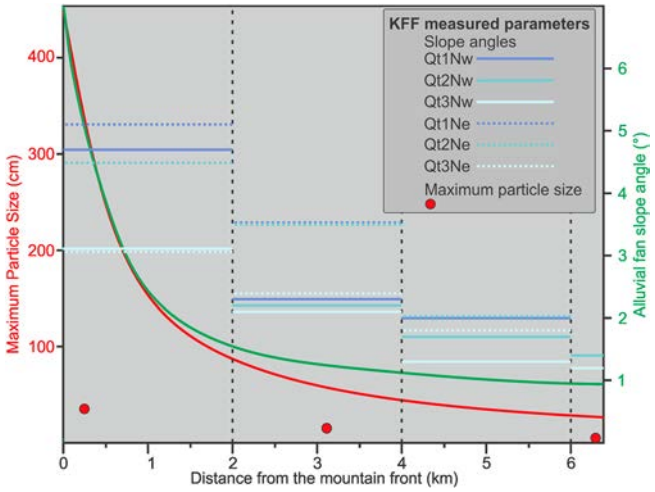

Figure 15. Obtained mean slope angle compared with maximum particle size of the KFF alluvial fans and with the mean fan surface slope angle (green), observed along the radial profile of alluvial fans in semiarid settings (curve after *Blissenbach* [1954]). The corresponding mean of maximum particle size values (red) is also reported for the same alluvial fans in semiarid settings (curve after *Blissenbach* [1954]).

Figure 14 shows the results of fan slope angle analysis for the three alluvial fan generations within the "west" and "east" areas (Figure 8a). The mean slope angle of the different alluvial fan generations are plotted with 1σ error bars. The segments corresponding to their average slope are plotted at their average elevation for the two selected areas, along four equal-spaced sectors (A, B, C, and D in Figure 8a) parallel to the CFS. The northing range of fault segments position is also indicated. The analysis clearly shows that there are differences in slope angle (fault-related tilting component) and elevation (channel downcutting component controlled also by drainage rearrangement) both between different fan generations (within the same sector) and between the two selected areas.

It might be argued that the different alluvial fan surface slope values could be biased by the overall grain size variability among the three fan generations and/or from the fan apex sectors to the distal portions. Nevertheless, the three generations of alluvial fan deposits exhibit similar maximum particle size for comparable distances from the mountain front (Figures 9e–9g). Furthermore, by comparing the obtained alluvial fan slope angle with those found on other alluvial fans in semiarid settings [e.g., *Blissenbach*, 1954], it is clear that our data consistently exceed the expected slope angles (Figure 15). Moreover, the observed maximum particle size of the KFF alluvial fans (~35 cm at the apex, ~15 cm in the central part, and ~5 cm in the distal part) seems to be much smaller than the expected one for the obtained slope values. This implies that the amount of longitudinal slope decrease for each fan generation cannot be completely ascribed to their possible original undisturbed convex-up shape but rather that postdepositional tilting has occurred.

The results of fan slope angle analysis (Figure 14) highlight the following patterns: (i) the average slope is generally greater for Qt1 fans and progressively decreases for Qt2 and Qt3 and (ii) statistically significant fan slope differences are recorded close to the faults, while such differences decrease proportionally away from faults. Differences in slope angle values are also recorded from west to east; specifically, (i) tilting and elevation of the three alluvial fan generations is greater in the "east" area; (ii) in the "west" area the tilting is recorded between the abandonments of Qt1w and Qt2w, whose profiles seem to be disturbed in the vicinity of an inferred fault at the end of Sector B (Figure 8a); and (iii) in the "east" area, Qt1e and Qt2e show approximately parallel slope profiles, though located at different elevations, and tilting is recorded between the abandonments of Qt2e and Qt3e.

6.2. Fluvial Terraces Along the EFS

Close to the northernmost branch of the EFS, the fill terrace architecture testifies to multiple cut-and-fill episodes (schematic section A in Figure 16a). There, no basal surfaces sculpted in the Neogene bedrock were entrenched by the river (Figures 10a and 10b) and the outcropping thickness of T1, T2, and T3 fill deposits is

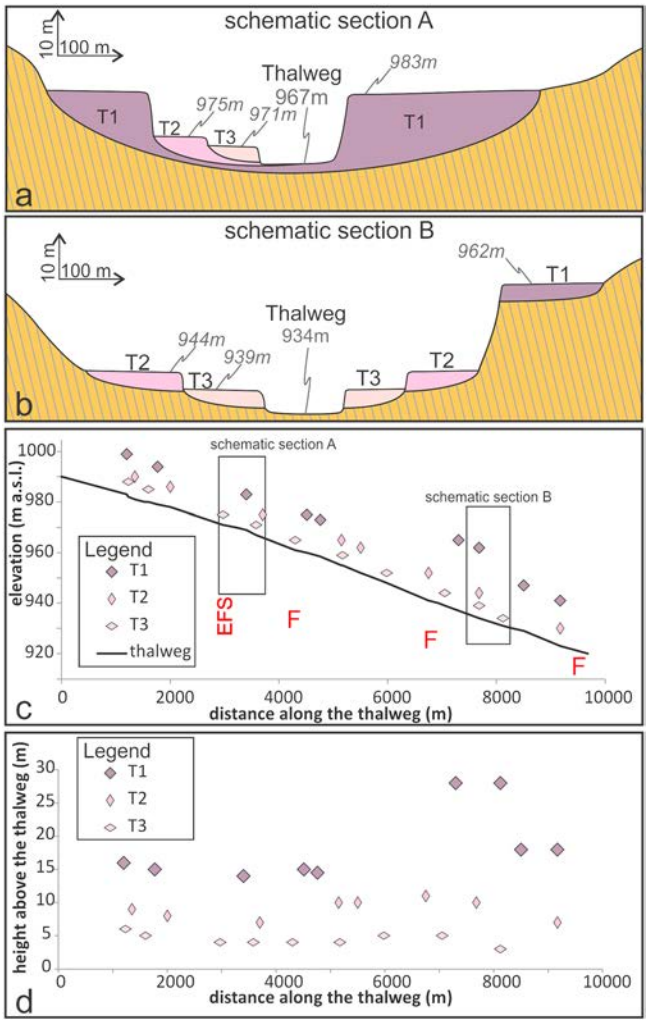

Figure 16. Fluvial terrace staircase setting in Zone 3. (a) Schematic section close to the main segment of the EFS; (b) schematic section close to the southernmost fault segments (see Figure 8 for the location of the schematic sections). (c) The remnants of the terrace top surfaces are projected along the river longitudinal profile, and (d) the longitudinal changes of the terrace height above the thalweg is also shown as evidence of changing river incision.

~14 m, ~8 m, and ~4 m, respectively (Figure 16a). Moving toward the southernmost fault segments (schematic section B in Figure 16b), changes in the terrace staircase architecture are considerable; notably, (i) the erosional basal surfaces of the T1 and T3 alluvial deposits, sculpted in the Neogene bedrock, are hanging above the thalweg 24 m and 2 m, respectively and (ii) the outcropping thicknesses of deposits in this section decrease to ~4 m for T1 (Figure 10c) and ~5 m for T2, while it remains constant at ~4 m for T3 (Figure 10d).

Furthermore, the elevation of the well-preserved remnants of fill terrace top surfaces projected on the present longitudinal profile (Figure 16c) locally bulges upward in the lower channel reach, particularly for T1. The terrace surface heights above the present thalweg (Figure 16d) plotted versus the distance along the channel profile seem to indicate that T2 and T3 also experienced a slight upward bulging within the same sector. However, the amount of bulging for T2 and T3 is too low to be significant. Nonetheless, an active response of the river to surface uplift after the abandonment of T3 is testified by the hanging of the basal erosional surface of the T3 deposit, which is sculpted into bedrock and lies 2 m above the thalweg (Figure 10d).

7. Discussion

The data set presented in this study provides new constraints on the timing and pattern of Quaternary activity of strike-slip fault systems at the northern edge of Lut Block. In particular, the OSL and structural data set on the Quaternary deposits along the KSF-KFF fault zone indicates that strike-slip fault activity and related localized uplift occurred post ~50 ka through Holocene times, with a general progression of fault zone localization and slip along eastward propagating KFF.

7.1. Topographic Inheritance and the Long-Term History of the KFF

A link can be found between the topographic signal, the punctuated exhumation history, and the style of deformation in the eastward propagating KFF system. Results from *Calzolari et al.* [2015] documented that the long-term Neogene growth of the KFF created a barrier to sediment flux from the DF ridge as well as a new source of sediments. This resulted in the accumulation of a thick pile of Neogene deposits around the developing KFF ridge. The progressive eastward topographic growth of the KFF deformation zone is confirmed by the northeastward increase of minimum topography of the range, which also corresponds to

a progressively higher relict base level of erosion, roughly corresponding to the paleopediment surface (Figures 9c and 9d). An eastward decrease in maximum topography is also recorded. This evidence suggests increasing denudation toward the east (decrease of the maximum topography), associated with eastward propagating rock uplift (increase of the minimum topography). This interpretation of progressively higher denudation toward the east is supported by the thick pile of Neogene sediments to the east (accompanying the first exhumation event), which are considerably more erodible than the basement units outcropping to the west [*Calzolari et al*., 2015].

A 10 km wavelength signal, corresponding to the ~42 km long western topographic domain, likely encompasses the remnant topographic fingerprint of both exhumation events (~18 Ma and ~4 Ma). The overall eastward narrowing, decrease of elevation and relief, and the ~23 km long eastern topographic domain can instead be identified as the remnant of the topographic signal of the second (~4 Ma) exhumation event. No syntectonic deposits are preserved in the proximity (tens of kilometers) of the KFF related to the second exhumation event at ~4 Ma, likely due to the formation of the regional paleopediment that cuts the tilted Neogene deposits. The ~4 Ma exhumation event and the pedimentation phase (favored by the exposure of the erodible Neogene units) caused the current outcrop of progressively deeper and localized fault zones to the east [*Calzolari et al*., 2015].

7.2. Tectonic Fingerprint in the Quaternary Geomorphic Signal

The inherited fault-related topographic arrangement of the KFF strongly conditioned the Quaternary drainage network evolution and the genesis of related landforms. Nonetheless, beyond the topographic control on drainage network development, rivers responded to both climatic and active tectonic forcing, which influenced the Quaternary erosion/deposition dynamics around the linear ridges.

From our field surveys we identified three generations of alluvial fans (Qt1 to Qt3) and river fill terraces (T1 to T3) that have been correlated and chronologically constrained to three age clusters of ~53, ~25, and ~6 ka, respectively. These ages are consistent with OSL and IRSL ages obtained regionally for the Quaternary alluvial fan deposits in Eastern Iran [*Walker and Fattahi*, 2011, and references therein] and with the ^{10}Be surface abandonment ages obtained by *Regard et al*. [2006], which unequivocally indicate that the alluvial deposition dynamics in the KSF and KFF areas is the result of Late Quaternary and Holocene wet climate-driven aggradation phases. Furthermore, the OSL ages constrain the timing of the dextral active faulting along the intraplate KSF and KFF deformation zones to the late Pleistocene-Holocene.

The lack of Quaternary deposits older than ~53 ka suggests also that the erosive phase that culminated with the paleopediment formation likely continued until the Late Pleistocene, implying a considerable sediment flux out of the KFF area. The paleopediment was successively entrenched, due to considerable drainage rearrangement and active deformation.

Local base-level changes produced both by drainage rearrangement and active tectonic deformation are mainly revealed by the architecture of the three alluvial fan and fill terrace generations developed around the KFF ridge. The telescopic arrangement of alluvial fans on the northern piedmont of the KFF ridge and the stacked arrangement on the southern one can be related to (i) the asymmetric growth of the ridge according to the position of the active fault strands; (ii) the rearrangement of the drainage network in response to local base-level changes.

We identified tectonic fingerprints on the Quaternary landforms by analyzing the alluvial fans and fluvial terraces as passive geomorphic markers. Because alluvial fans apexes are located on the margin of the fault-bounded deformation zone, these geomorphic markers do not show strike-slip offsets, although late Quaternary faulting was constrained through OSL dating. Nonetheless, the topographic arrangement of the geomorphic markers allowed us to detect perturbations associated with localized fault-related uplift along the KFF. Statistical alluvial fan slope analysis performed across the CFS documents a progressive tilting of the alluvial fan surfaces, which cannot be explained by processes other than fault-related uplift during the late Quaternary-to-Holocene time span. The fact that the tilting generally decreases away from the principal fault (CFS) and vanishes at the end of sector C (Figure 8) indicates that the fault itself is the driver of such tilting. Fault-related tilting seems to have occurred through localized and diachronous deformation from west to east, as testified by the different degree of tilting for different fan generations in the two analyzed sectors (Figure 14b).

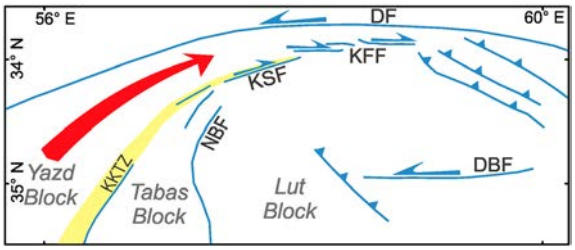

Figure 17. A possible kinematic scenario for the post-Neogene strike-slip fault architecture at the northern margin of Lut Block (modified after *Nozaem et al.* [2013]). The present and concurrent activity of sinistral and dextral systems along subparallel fault strands suggests that their opposite kinematics are governed by a relative westward, lateral extrusion (red arrow) of the tectonic block delimited by the DF and the KSF-KFF systems. DF: Doruneh Fault, KSF: Kuh-e-Sarhangi Fault, KFF: Kuh-e-Faghan Fault, NBF: Nayband Fault, DBF: Dasht-e-Bayaz Fault, KKTZ: Kashmar-Kerman Tectonic Zone (in yellow).

We have documented that localized fault-related uplift is active (postdates the abandonment of the T3 terrace) also along the fault segments to the south of the EFS, as testified by the architecture of fill terraces. The variability of both terrace height and thickness of the three generations of Late Quaternary fill terraces along the river profile suggests that the river responded to localized uplift in the vicinity of fault segments to the south of the EFS through locally increased incision and decreased thickness of the terrace deposits. The latter is more evident for T1 terrace. Furthermore, after the abandonment of the T1 terrace, its top surface became a passive geomorphic marker that continued to record a bulging due to the active fault-related localized uplift.

7.3. Implications for the Kinematic Configuration of Central Iran

Results of this study document that the northern edge of Lut Block is bounded by a dextral deformation belt active throughout late Quaternary times. Similar to major active regional strike-slip fault zones [e.g., *Schwartz and Coppersmith*, 1984; *Barka and Kadinsky-Cade*, 1988; *Wesnousky*, 1988, 2006; *Scholz*, 1990; *Lettis et al*., 2002; *Langridge et al*., 2002], the reconstructed fault pattern documents geometrical segmentation of the KSF-KFF system along a cumulative length of ~ 200 km. This active strike-slip deformation belt is localized along the northeastward termination of the Kashmar-Kerman tectonic zone (Figure 1), suggesting polyphase reactivation of structurally inherited discontinuities during Neogene-Quaternary times.

Despite that no direct evidence is provided on the actual slip rates along the KSF-KFF fault zone, a kinematic connection with the subparallel, sinistral Doruneh Fault (Figures 1 and 2) is indicated by the concurrent Quaternary activity of both fault systems [*Tchalenko et al*., 1973; *Fattahi et al*., 2007; *Farbod et al*., 2011; *Javadi et al*., 2013; *Nozaem et al*., 2013; *Calzolari et al*., 2015; *Khodaverdian et al*., 2015; this study]. In particular, the concurrent activity of the sinistral DF and the dextral KSF-KFF systems along subparallel fault strands during the Quaternary suggests that their opposite kinematics are governed by a relative westward, lateral extrusion of the tectonic block delimited by these fault systems (Figure 17) [see also *Nozaem et al*., 2013]. Such escape component seems to be supported by the GPS data for Central Iran [*Walpersdorf et al*., 2014] (Figure 1), which show that the Yazd Block is moving northward at faster velocities with respect to the areas lying to its east and west. The lateral escape of the Yazd Block and Tabas Block toward Lut Block along the Nayband Fault (Figure 1) has been also proposed as a component of the seismotectonic scenario of Central Iran by *Bonini et al*. [2003].

The escape tectonic scenario is at odds with the current kinematic configuration proposed for Central Iran, commonly framed into a scenario of dynamic rupture achieved through a set of conjugate N-S dextral and E-W sinistral slip zones, associated with rigid block rotations and strain partitioning [e.g., *Allen et al*., 2004; *Walker and Jackson*, 2004; *Mattei et al*., 2012; *Walpersdorf et al*., 2014]. In particular, modeling GPS data with a block rotation model suggests that the rotations have been going on at a similar rate ($1 \pm 0.4°$/Ma) over the last 12 Ma [*Walpersdorf et al*., 2014]. Nonetheless, this timing for the initiation of this rigid block rotation scenario is in disagreement with the estimated ~5 to ~7 Ma onset of strike-slip tectonics in south Central Iran [*Allen et al*., 2004, 2011; *Walker and Jackson*, 2004]. Finally, the rigid block rotation model contrasts with the Neogene-Quaternary kinematic configuration recently recognized for the northern boundary of Lut Block, where punctuated events of fault zone (re)activation and space-time kinematic shifts have been documented for the Neogene-Quaternary time lapse [*Farbod et al*., 2011; *Javadi et al*., 2013; *Nozaem et al*., 2013; *Calzolari et al*., 2015; this study].

Although the ultimate cause for the new kinematic configuration at the northern edge of the CEIM is open for debate and beyond the scope of this study, we think a kinematic model dominated by crustal thickening and

lateral extrusion of the Yazd Block in Central Iran during the Arabia-Eurasia collision better fits the new kinematics findings and temporal evolution of deformation along the northern margin of Lut Block (Figure 17). The dynamic scenario to accomplish for this new hypothesis resides in the idea that a gradual decrease in the capacity to accommodate convergence along the Zagros collisional zone since the Pliocene [*Allen et al*., 2004; *Austermann and Iaffaldano*, 2013] resulted in an overall advancing convergent plate margin, with a further increase in the intraplate residual convergence. In Central Iran, this new kinematic configuration led to northward convergence velocities that decreased away from the Zagros-Makran Transfer Zone. This later kinematic configuration remained unchanged since then. Evidence provided by the GPS data, showing northward convergence vectors that generally decrease away from (to the northwest and east of) the Zagros-Makran Transfer Zone [*Vernant et al*., 2004; *Walpersdorf et al*., 2014] (Figure 1) may confirm this reconstruction.

8. Conclusions

The main results of this study can be summarized as follows:

1. The present topographic signal of the KFF is likely the inherited remnant of the Neogene punctuated history of fault nucleation, propagation, and exhumation, and it reflects the style of deformation within the fault system. Such inherited topography influenced the Quaternary drainage network evolution and thus the Quaternary erosion/deposition dynamics around the linear ridge.
2. Three generations of Quaternary alluvial fans and river fill terraces associated with the dismantling of the fault-related topographic relief were recognized and dated by means of OSL at ~53, ~25, and ~6 ka, respectively. They are well correlated with the regionally defined Late Quaternary aggradation and abandonment phases previously recognized over Central Eastern Iran in other studies. Such dates constrain to the Holocene the minimum age of faulting along the KSF-KFF dextral strike-slip system at the northern edge of Lut Block (Central Iran).
3. Alluvial fan and fluvial terrace architecture was controlled by base-level changes due to both drainage network rearrangement and fault-related deformation. The latter was isolated through the quantitative analysis of the topographic arrangement of alluvial fans and fluvial terraces as passive geomorphic markers, which recorded localized uplift along the single fault strands of the KFF.
4. A new kinematic model for the Quaternary and active faulting in Central Iran is thus necessary. Crustal thickening and lateral extrusion of the Yazd Block during progress of the Arabia-Eurasia collision may provide a feasible scenario.

Acknowledgments

Special thanks go to M.R. Mazinini for assistance during field work. Manager and staff of Khaney-e-Moallem of Kashmar are warmly thanked for their kind hospitality. We also thank Ali Rastpour and Hassan Faraji for driving to the field and logistic support. We are grateful to P. Ballato and to an anonymous referee for their critical review of the manuscript. Special thanks are reserved for the Associate Editor, T. Schildgen, for her precious comments and for her considerable efforts to make the paper improved. This project has been funded by TOPOMOD Marie Curie ITN project (grant agreement 264517). Authors will curate the above data for at least 5 years after publication and provide a transparent process to make the data available to anyone upon request, with any restrictions on access.

References

Agard, P., J. Omrani, L. Jolivet, H. Whitechurch, B. Vrielynck, W. Spakman, P. Monié, B. Meyer, and R. Wortel (2011), Zagros orogeny: A subduction-dominated process, *Geol. Mag.*, *148*(5–6), 692–725, doi:10.1017/s001675681100046x.

Aghanabati, A. (2004), *Geology of Iran*, Geol. Surv. of Iran, Tehran.

Allen, C. R. (1965), Transcurrent faults in continental areas, *Philos. Trans. R. Soc. London A*, *258*, 82–89, doi:10.1098/rsta.1965.0023.

Allen, M. B., J. Jackson, and R. Walker (2004), Late Cenozoic reorganization of the Arabia-Eurasia collision and the comparison of short-term and long-term deformation rates, *Tectonics*, *23*, TC2008, doi:10.1029/2003TC001530.

Allen, M. B., M. Kheirkhah, M. H. Emami, and S. J. Jones (2011), Right-lateral shear across Iran and kinematic change in the Arabia-Eurasia collision zone, *Geophys. J. Int.*, *184*(2), 555–574, doi:10.1111/j.1365-246X.2010.04874.x.

Austermann, J., and G. Iaffaldano (2013), The role of the Zagros orogeny in slowing down Arabia-Eurasia convergence since ~5 Ma, *Tectonics*, *32*, 351–363, doi:10.1002/tect.20027.

Avouac, J. P., P. Tapponnier, M. Bai, H. You, and G. Wang (1993), Active thrusting and folding along the northeastern Tien Shan and late Cenozoic rotation of Tarim with respect to Dzungaria and Kazakhstan, *J. Geophys. Res.*, *98*, 6755–6804, doi:10.1029/92JB01963.

Barka, A., and K. Kadinsky-Cade (1988), Strike-slip fault geometry in Turkey and its influence on earthquake activity, *Tectonics*, *7*, 663–684, doi:10.1029/TC007i003p00663.

Beaumont, P. (1972), Alluvial fans along the foothills of the Elburz Mountains, Iran, *Palaeogeogr. Palaeoclimatol. Palaeoecol.*, *12*, 251–273, doi:10.1016/0031-0182(72)90022-3.

Belisario, F., M. Del Monte, P. Fredi, R. Funiciello, E. Lupia Palmieri, and F. Salvini (1999), Azimuthal analysis of stream orientations to define regional tectonic lines, *Z. Geomorphol. Suppl. Bd.*, *118*, 41–63.

Bennett, E. R., J. H. Youngson, J. A. Jackson, R. J. Norris, G. M. Raisbeck, and F. Yiou (2006), Combining geomorphic observations with in-situ cosmogenic isotope measurements to study anticline growth and fault propagation in Central Otago, New Zealand, *N. Z. J. Geol. Geophys.*, *49*, 217–231, doi:10.1080/00288306.2006.9515161.

Berberian, M. (1976), First seismotectonic map of Iran, 1:2,500,000, in *Contribution to the Seismotectonics of Iran, Part II*, edited by M. Berberian, Geol. Surv. Iran Rep. 39, Tehran.

Berberian, M. (1977), Historical seismicity (Pre 1900) map of Iran, 1:5,000,000, in *Contribution to the Seismotectonics of Iran, Part III*, edited by M. Berberian, Geol. Min. Surv. Iran Rep. 40, Tehran.

Berberian, M. (2014), *Earthquakes and Coseismic Surface Faulting on the Iranian Plateau*, Elsevier Sci., Amsterdam, Netherlands.

Berberian, M., and G. King (1981), Towards a paleogeography and tectonic evolution of Iran, *Can. J. Earth Sci.*, *18*(2), 210–265, doi:10.1139/e81-019.
Blissenbach, E. (1954), Geology of alluvial fans in semiarid regions, *Geol. Soc. Am. Bull.*, *65*(2), 175–190, doi:10.1130/0016-7606(1954)65[175:GOAFIS]2.0.CO;2.
Bonini, M., G. Corti, D. Sokoutis, G. Vannucci, P. Gasperini, and S. Cloetingh (2003), Insights from scaled analogue modelling into the seismotectonics of the Iranian region, *Tectonophysics*, *376*, 137–149.
Bookhagen, B., and M. R. Strecker (2012), Spatiotemporal trends in erosion rates across a pronounced rainfall gradient: Examples from the southern Central Andes, *Earth Planet. Sci. Lett.*, *327–328*, 97–110, doi:10.1016/j.epsl.2012.02.005.
Bridgland, D. R. (2000), River terrace systems in north-west Europe: An archive of environmental change, uplift and early human occupation, *Quat. Sci. Rev.*, *19*(13), 1293–1303, doi:10.1016/S0277-3791(99)00095-5.
Bridgland, D. R., and R. Westaway (2008), Climatically controlled river terrace staircases: A worldwide Quaternary phenomenon, *Geomorphology*, *98*, 285–315, doi:10.1016/j.geomorph.2006.12.032.
Bull, W. B. (1977), The alluvial-fan environment, *Prog. Phys. Geogr.*, *1*, 222–270.
Bull, W. B. (2007), *Tectonic Geomorphology of Mountains: A New Approach to Paleoseismology*, Blackwell, Oxford, U. K.
Bull, W. B. (2009), *Tectonically Active Landscapes*, John Wiley, Chichester, West Sussex, U. K.
Burbank, D. W., and R. S. Anderson (2012), *Tectonic Geomorphology*, John Wiley, Chichester, West Sussex, U. K.
Calzolari, G., F. Rossetti, M. Della Seta, R. Nozaem, V. Olivetti, M. L. Balestrieri, D. Cosentino, C. Faccenna, F. M. Stuart, and G. Vignaroli (2015), Spatio-temporal evolution of intraplate strike-slip faulting: The Neogene-Quaternary Kuh-e-Faghan fault, Central Iran, *Geol. Soc. Am. Bull.*, doi:10.1130/B31266.1.
Castelltort, S., L. Goren, S. D. Willett, J. D. Champagnac, F. Herman, and J. Braun (2012), River drainage patterns in the New Zealand Alps primarily controlled by plate tectonic strain, *Nat. Geosci.*, *5*, 744–748, doi:10.1038/NGEO1582.
Cooke, R., A. Warren, and A. Goudie (1993), *Desert Geomorphology*, Univ. Coll. of London Press, London.
D'Agostino, N., and D. McKenzie (1999), Convective support of long-wavelength topography in the Apennines (Italy), *Terra Nova*, *11*, 228–233, doi:10.1046/j.1365-3121.1999.00252.x.
Della Seta, M., M. Del Monte, P. Fredi, and E. Lupia Palmieri (2004), Quantitative morphotectonic analysis as a tool for detecting deformation patterns in soft-rock terrains: A case study from the southern Marches, Italy, *Geomorphologie*, *4*, 267–284, doi:10.3406/morfo.2004.1224.
Della Seta, M., M. Del Monte, P. Fredi, E. Miccadei, O. Nesci, G. Pambianchi, T. Piacentini, and F. Troiani (2008), Morphotectonic evolution of the Adriatic piedmont of the Apennines: An advancement in the knowledge of the Marche-Abruzzo border area, *Geomorphology*, *102*(1), 119–129, doi:10.1016/j.geomorph.2007.06.018.
Dohrenwend, J., and A. Parsons (2009), Pediments in arid environments, in *Geomorphology of Desert Environments*, edited by A. Parsons and A. Abrahams, pp. 377–411, Springer, Dordrecht, Netherlands.
Dufaure, J. J., C. Thibault, M. H. Kadjar, and J. L. Mercier (1978), La zone de failles du Zendan (Iran du Sud-Est): I-Géomorphologie et Stratigraphie du Quaternaire, paper presented at Réunion Annuelle des Sciences de la Terre (6th RAST), Soc. Geol. de France, Orsay, France.
Eftekhar-Nezhad, J., A. Aghanabati, B. Hamzehpour, and V. Baroyant (1976), 1:250,000 scale, Geol. Surv. of Iran, Kashmar.
Farbod, Y., O. Bellier, E. Shabanian, and M. R. Abbassi (2011), Geomorphic and structural variations along the Doruneh Fault System (Central Iran), *Tectonics*, *30*, TC6014, doi:10.1029/2011TC002889.
Fattahi, M., R. T. Walker, M. M. Khatib, A. Dolati, and A. Bahroudi (2007), Slip-rate estimate and past earthquakes on the Doruneh fault, Eastern Iran, *Geophys. J. Int.*, *168*(2), 691–709, doi:10.1111/j.1365-246X.2006.03248.x.
Foroutan, M., et al. (2014), Late Pleistocene-Holocene right slip rate and paleoseismology of the Nayband fault, western margin of Lut block, Iran, *J. Geophys. Res. Solid Earth*, *119*, 3517–3560, doi:10.1002/2013JB010746.
Fubelli, G., M. Della Seta, and G. Amato (2014), Drainage system adjustment in response to the opening of the Rieti intermontane basin (Central Italy): Geostatistical reconstruction of the PaleoFarfa River alluvial plain, *Rend. Lincei Sci. Fis. Nat.*, *25*(Suppl. 2), 167–176, doi:10.1007/s12210-014-0322-0.
Giano, S. I. (2011), Quaternary alluvial fan systems of the Agri intermontane basin (southern Italy): Tectonic and climatic controls, *Geol. Carpath.*, *62*(1), 65–76, doi:10.2478/v10096-011-0006-y.
Giano, S. I., D. Gioia, and M. Schiattarella (2014), Morphotectonic evolution of connected intermontane basins from the southern Apennines, Italy: The legacy of the pre-existing structurally controlled landscape, *Rend. Lincei Sci. Fis. Nat.*, *25*(Suppl. 2), 241–252, doi:10.1007/s12210-014-0325-x.
Gioia, D., S. Gallicchio, M. Moretti, and M. Schiattarella (2014), Landscape response to tectonic and climatic forcing in the foredeep of the southern Apennines, Italy: Insights from Quaternary stratigraphy, quantitative geomorphic analysis, and denudation rate proxies, *Earth Surf. Processes Landforms*, *39*(6), 814–835, doi:10.1002/esp.3544.
Hancock, G. S., and R. S. Anderson (2002), Numerical modeling of fluvial strath-terrace formation in response to oscillating climate, *Geol. Soc. Am. Bull.*, *114*(9), 1131–1142, doi:10.1130/0016-7606(2002)114<1131:NMOFST>2.0.CO;2.
Harvey, A. M. (1997), The role of alluvial fans in arid zone fluvial systems, in *Arid Zone Geomorphology; Process, Form and Change in Drylands*, edited by D. S. G. Thomas, pp. 231–259, Wiley, Chichester, U. K.
Hatzfeld, D., and P. Molnar (2010), Comparisons of the kinematics and deep structures of the Zagros and Himalaya and of the Iranian and Tibetan plateaus and geodynamic implications, *Rev. Geophys.*, *48*, RG2005, doi:10.1029/2009RG000304.
Hergarten, S., J. Robl, and K. Stüwe (2014), Extracting topographic swath profiles across curved geomorphic features, *Earth Surf. Dyn.*, *2*, 97–104, doi:10.5194/esurf-2-97-2014.
Hessami, K., F. Jamali, and H. Tabassi (2003), *Major Active Faults of Iran*, Int. Inst. of Earthquake Eng. and Seismol. of Iran Press, Tehran.
Homke, S., J. Vergés, P. Van Der Beek, M. Fernàndez, E. Saura, L. Barbero, B. Badics, and E. Labrin (2010), Insights in the exhumation history of the NW Zagros from bedrock and detrital apatite fission-track analysis: Evidence for a long-lived orogeny, *Basin Res.*, *22*(5), 659–680.
Hubert-Ferrari, A., R. Armijo, G. King, B. Meyer, and A. Barka (2002), Morphology, displacement, and slip rates along the North Anatolian Fault, Turkey, *J. Geophys. Res.*, *107*(B10), 2235, doi:10.1029/2001JB000393.
Hutchinson, M. F., T. Xu, and J. A. Stein (2011), Recent progress in the ANUDEM elevation gridding procedure, *Conference Paper in Geomorphometry 2011*, edited by T. Hengel et al., pp. 19–22, Redlands, Calif. [Available at http://geomorphometry.org/HutchinsonXu2011.]
Jackson, J., A. Haines, and A. Holt (1995), The accommodation of the Arabia–Eurasia plate convergence in Iran, *J. Geophys. Res.*, *100*, 15,205–15,219, doi:10.1029/95JB0129.
Jackson, J., R. Norris, and J. Youngson (1996), The structural evolution of active fault and fold systems in central Otago, New Zealand: Evidence revealed by drainage patterns, *J. Struct. Geol.*, *18*, 217–234, doi:10.1016/S0191-8141(96)80046-0.

Javadi, H. R., M. R. Ghassemi, M. Shahpasandzadeh, B. Guest, M. E. Ashtiani, A. L. I. Yassaghi, and M. Kouhpeyma (2013), History of faulting on the Doruneh Fault System: Implications for the kinematic changes of the Central Iranian Microplate, *Geol. Mag.*, *150*(4), 651–672, doi:10.1017/s0016756812000751.

Javadi, H. R., M. Esterabi Ashtiani, B. Guest, A. Yassaghi, M. R. Ghassemi, M. Shahpasandzadeh, and A. Naeimi (2015), Tectonic reversal of the western Doruneh Fault System: Implications for Central Asian tectonics, *Tectonics*, *34*, doi:10.1002/2015TC003931.

Jolivet, L., and C. Faccenna (2000), Mediterranean extension and the Africa-Eurasia collision, *Tectonics*, *19*, 1095–1106, doi:10.1029/2000TC900018.

Khodaverdian, A., H. Zafarani, and M. Rahimian (2015), Long term fault slip rates, distributed deformation rates and forecast of seismicity in the Iranian Plateau, *Tectonics*, *34*, doi:10.1002/2014TC003796.

Langridge, R. M., H. D. Stenner, T. E. Fumal, S. A. Christofferson, T. K. Rockwell, R. D. Hartleb, J. Bachhuber, and A. A. Barka (2002), Geometry, slip distribution, and kinetics of surface rupture on the Sakarya fault segment during the 17 August 1999 Izmit, Turkey, earthquake, *Bull. Seismol. Soc. Am.*, *92*(1), 107–125, doi:10.1785/0120000804.

Lavé, J., and J. P. Avouac (2001), Fluvial incision and tectonic uplift across the Himalayas of central Nepal, *J. Geophys. Res.*, *106*, 26,561–26,591, doi:10.1029/2001JB000359.

Lettis, W., J. Bachhuber, R. Witter, C. Brankman, C. E. Randolph, A. Barka, W. D. Page, and A. Kaya (2002), Influence of releasing stepovers on surface fault rupture and fault segmentation: Examples from the 17 August 1999 Izmit earthquake on the North Anatolian Fault, Turkey, *Bull. Seismol. Soc. Am.*, *92*(1), 19–42, doi:10.1785/0120000808.

Madanipour, S., T. A. Ehlers, A. Yassaghi, M. Rezaeian, E. Enkelmann, and A. Bahroudi (2013), Synchronous deformation on orogenic plateau margins: Insights from the Arabia–Eurasia collision, *Tectonophysics*, *608*, 440–451, doi:10.1016/j.tecto.2013.09.003.

Maddy, D., D. Bridgland, and R. Westaway (2001), Uplift-driven valley incision and climate-controlled river terrace development in the Thames Valley, UK, *Quat. Int.*, *79*, 23–36, doi:10.1016/S1040-6182(00)00120-8.

Mattei, M., F. Cifelli, G. Muttoni, A. Zanchi, F. Berra, F. Mossavvari, and S. A. Eshraghi (2012), Neogene block rotation in Central Iran: Evidence from paleomagnetic data, *Geol. Soc. Am. Bull.*, *124*(5–6), 943–956, doi:10.1130/B30479.1.

McClusky, S., R. Reilinger, S. Mahmoud, D. B. Sari, and A. Tealeb (2003), GPS constraints on Africa (Nubia) and Arabia plate motions, *Geophys. J. Int.*, *155*, 126–138, doi:10.1046/j.1365-246X.2003.02023.x.

Mitchell, S. G., and D. R. Montgomery (2006), Influence of a glacial buzzsaw on the height and morphology of the Washington Cascade Range, Washington State, USA, *Quat. Res.*, *65*(1), 96–107, doi:10.1016/j.yqres.2005.08.018.

Molin, P., F. J. Pazzaglia, and F. Dramis (2004), Geomorphic expression of active tectonics in a rapidly-deforming forearc, Sila Massif, Calabria, Southern Italy, *Am. J. Sci.*, *304*(7), 559–589, doi:10.2475/ajs.304.7.559.

Molin, P., G. Fubelli, M. Nocentini, S. Sperini, P. Ignat, F. Grecu, and F. Dramis (2012), Interaction of mantle dynamics, crustal tectonics, and surface processes in the topography of the Romanian Carpathians: A geomorphological approach, *Global Planet. Change*, *90*, 58–72, doi:10.1016/j.gloplacha.2011.05.005.

Mouthereau, F., O. Lacombe, and J. Vergés (2012), Building the Zagros collisional orogen: Timing, strain distribution and the dynamics of Arabia/Eurasia plate convergence, *Tectonophysics*, *532–535*, 27–60, doi:10.1016/j.tecto.2012.01.022.

Nilforoushan, F., et al. (2003), GPS network monitors the Arabia-Eurasia collision deformation in Iran, *J. Geod.*, *77*(7–8), 411–422, doi:10.1007/s00190-003-0326-5.

Nozaem, R., M. Mohajjel, F. Rossetti, M. Della Seta, G. Vignaroli, A. Yassaghi, F. Salvini, and M. Eliassi (2013), Post-Neogene right-lateral strike-slip tectonics at the north-western edge of the Lut Block (Kuh-e–Sarhangi Fault), Central Iran, *Tectonophysics*, *589*, 220–233, doi:10.1016/j.tecto.2013.01.001.

Pérez-Peña, J. V., J. M. Azañón, A. Azor, J. Delgado, and F. González-Lodeiro (2009a), Spatial analysis of stream power using GIS: SLk anomaly maps, *Earth Surf. Processes Landforms*, *34*, 16–25, doi:10.1002/esp.1684.

Pérez-Peña, J. V., J. M. Azañón, and A. Azor (2009b), CalHypso: An ArcGIS extension to calculate hypsometric curves and their statistical moments. Applications to drainage basin analysis in SE Spain, *Comput. Geosci.*, *35*(6), 1214–1223, doi:10.1016/j.cageo.2008.06.006.

Ramezani, J., and R. D. Tucker (2003), The Saghand region, Central Iran: U-Pb geochronology, petrogenesis and implications for Gondwana tectonics, *Am. J. Sci.*, *303*(7), 622–665, doi:10.2475/ajs.303.7.622.

Regard, V., O. Bellier, R. Braucher, F. Gasse, D. Bourlès, J. Mercier, J. C. Thomas, M. R. Abbassi, E. Shabanian, and S. Soleymani (2006), ^{10}Be dating of alluvial deposits from Southeastern Iran (the Hormoz Strait area), *Palaeogeogr. Palaeoclimatol. Palaeoecol.*, *242*(1–2), 36–53, doi:10.1016/j.palaeo.2006.05.012.

Reilinger, R., et al. (2006), GPS constraints on continental deformation in the Africa-Arabia-Eurasia continental collision zone and implications for the dynamics of plate interactions, *J. Geophys. Res.*, 111, B05411, doi:10.1029/2005JB004051.

Replumaz, A., R. Lacassin, P. Tapponnier, and P. H. Leloup (2001), Large river offsets and Plio-Quaternary dextral slip rate on the Red River fault (Yunnan, China), *J. Geophys. Res.*, *106*, 819–836, doi:10.1029/2000JB900135.

Rockwell, T. K., K. A. Keller, M. N. Clark, and D. L. Johnson (1984), Chronology and rates of faulting of Ventura River terraces, California, *Geol. Soc. Am. Bull.*, *95*, 1466–1474, doi:10.1130/0016-7606(1984)95<1466:CAROFO>2.0.CO;2.

Rossetti, F., R. Nozaem, F. Lucci, G. Vignaroli, A. Gerdes, M. Nasrabadi, and T. Theye (2015), Tectonic setting and geochronology of the Cadomian (Ediacaran-Cambrian) magmatism in Central Iran, Kuh-e-Sarhangi region (NW Lut Block), *J. Asian Earth Sci.*, *102*, 24–44, doi:10.1016/j.jseaes.2014.07.034.

Royden, L., and J. T. Perron (2013), Solutions of the stream power equation and application to the evolution of river longitudinal profiles, *J. Geophys. Res. Earth Surf.*, *118*, 497–518, doi:10.1002/jgrf.20031.

Ruttner, A., M. H. Nabavi, and M. Alavi (1970), *Geological Map of Ozbak Kuh Mountain (1/100,000)*, Geol. Surv. of Iran, Tehran.

Sahandi, M. R., M. R. Ghassemi, and Y. Ekhtiarabadi (2010), *Geological Map of Ghasemabad (1:100,000)*, Geol. Surv. of Iran, Tehran.

Salvini, F. (2004), Daisy 3 the structural data integrated system analyzer, Software Univ. of Roma Tre, Roma. [Available at http://host.uniroma3.it/progetti/fralab.]

Schiattarella, M., P. Di Leo, P. Beneduce, S. I. Giano, and C. Martino (2006), Tectonically driven exhumation of a young orogen: An example from southern Apennines, Italy, in *Tectonics, Climate, and Landscape Evolution*, *Spec. Pap., 398, Penrose Conf. Ser.*, edited by S. D. Willett et al., pp. 371–385, Geol. Soc. Am., Boulder, Colo., doi:10.1130/2006.2398(23).

Schildgen, T. F., D. Cosentino, B. Bookhagen, S. Niedermann, C. Yildirim, H. Echtler, H. Wittmann, and M. R. Strecker (2012), Multi-phased uplift of the southern margin of the Central Anatolian plateau, Turkey: A record of tectonic and upper mantle processes, *Earth Planet. Sci. Lett.*, *317–318*, 85–95, doi:10.1016/j.epsl.2011.12.003.

Scholz, C. H. (1990), *The Mechanics of Earthquakes and Faulting*, Cambridge Univ. Press, Cambridge, U. K.

Schumm, S. A. (1977), *The Fluvial System*, 388 pp., Wiley, New York.

Schwartz, D. P., and K. J. Coppersmith (1984), Fault behavior and characteristic earthquakes: Examples from the Wasatch and San Andreas Fault Zones, *J. Geophys. Res.*, *89*, 5681–5698, doi:10.1029/JB089iB07p05681.

Scotti, V. N., P. Molin, C. Faccenna, M. Soligo, and A. Casas-Sainz (2013), The influence of surface and tectonic processes on landscape evolution of the Iberian Chain (Spain): Quantitative geomorphological analysis and geochronology, *Geomorphology*, *206*, 37–57, doi:10.1016/j.geomorph.2013.09.017.

Sella, G. F., T. H. Dixon, and A. Mao (2002), REVEL: A model for recent plate velocities from space geodesy, *J. Geophys. Res.*, *107*(B4), 2081, doi:10.1029/2000JB000033

Strecker, M. R., P. Cerveny, A. L. Bloom, and D. Malizia (1989), Late Cenozoic tectonism and landscape development in the foreland of the Andes: Northern Sierras Pampeanas (26°–28°S), Argentina, *Tectonics*, *8*, 517–534, doi:10.1029/TC008i003p00517.

Talebian, M., and J. Jackson (2002), Offset on the main recent fault of NW Iran and implications for the late Cenozoic tectonics of the Arabia–Eurasia collision zone, *Geophys. J. Int.*, *150*, 422–439, doi:10.1046/j.1365-246X.2002.01711.x.

Talebian, M., and J. Jackson (2004), A reappraisal of earthquake focal mechanisms and active shortening in the Zagros mountains of Iran, *Geophys. J. Int.*, *156*, 506–526, doi:10.1111/j.1365-246X.2004.02092.x.

Tchalenko, J., M. Berberian, and H. Behzadi (1973), Geomorphic and seismic evidence for recent activity on the Doruneh Fault, Iran, *Tectonophysics*, *19*(4), 333–341, doi:10.1016/0040-1951(73)90027-9.

Telbisz, T., G. Kovács, B. Székely, and J. Szabó (2013), Topographic swath profile analysis: A generalization and sensitivity evaluation of a digital terrain analysis tool, *Z. Geomorphol.*, *57*(4), 485–513, doi:10.1127/0372-8854/2013/0110.

Troiani, F., and M. Della Seta (2008), The use of the Stream Length-Gradient Index in morphotectonic analysis of small catchments: A case study from central Italy, *Geomorphology*, *102*, 159–168, doi:10.1016/j.geomorph.2007.06.020.

Troiani, F., and M. Della Seta (2011), Geomorphological response of fluvial and coastal terraces to Quaternary tectonics and climate as revealed by geostatistical topographic analysis, *Earth Surf. Processes Landforms*, *36*(9), 1193–1208, doi:10.1002/esp.2145.

Vandenberghe, J. (2003), Climate forcing of fluvial system development: An evolution of ideas, *Quat. Sci. Rev.*, *22*(20), 2053–2060, doi:10.1016/S0277-3791(03)00213-0.

Vernant, P., et al. (2004), Present-day crustal deformation and plate kinematics in the Middle East constrained by GPS measurements in Iran and northern Oman, *Geophys. J. Int.*, *157*(1), 381–398, doi:10.1111/j.1365-246X.2004.02222.x.

Walker, R. T., and M. Fattahi (2011), A framework of Holocene and Late Pleistocene environmental change in Eastern Iran inferred from the dating of periods of alluvial fan abandonment, river terracing, and lake deposition, *Quat. Sci. Rev.*, *30*(9), 1256–1271, doi:10.1016/j.quascirev.2011.03.004.

Walker, R. T., and J. Jackson (2002), Offset and evolution of the Gowk fault, S.E. Iran: A major intra-continental strike-slip system, *J. Struct. Geol.*, *24*(11), 1677–1698, doi:10.1016/S0191-8141(01)00170-5.

Walker, R. T., and J. Jackson (2004), Active tectonics and late Cenozoic strain distribution in Central and Eastern Iran, *Tectonics*, *23*, TC5010, doi:10.1029/2003TC001529.

Walpersdorf, A., et al. (2014), Present-day kinematics and fault slip rates in Eastern Iran, derived from 11 years of GPS data, *J. Geophys. Res. Solid Earth*, *119*, 1359–1383, doi:10.1002/2013JB010620.

Wegmann, K. W., and F. J. Pazzaglia (2009), Late Quaternary fluvial terraces of the Romagna and Marche Apennines, Italy: Climatic, lithologic, and tectonic controls on terrace genesis in an active orogen, *Quat. Sci. Rev.*, *28*(1–2), 137–165, doi:10.1016/j.quascirev.2008.10.006.

Wegmann, K. W., B. D. Zurek, C. A. Regalla, D. Bilardello, J. L. Wollenberg, S. E. Kopczynski, J. M. Ziemann, S. L. Haight, J. D. Apgar, and C. Zhao (2007), Position of the Snake River watershed divide as an indicator of geodynamic processes in the greater Yellowstone region, western North America, *Geosphere*, *3*(4), 272–281, doi:10.1130/GES00083.1.

Wesnousky, S. G. (1988), Seismological and structural evolution of strike-slip faults, *Nature*, *335*, 340–343, doi:10.1038/335340a0.

Wesnousky, S. G. (2006), Predicting the endpoints of earthquake ruptures, *Nature*, *444*, 358–360, doi:10.1038/nature05275.

Westaway, R., M. Pringle, S. Yurtmen, T. Demir, D. Bridgland, G. Rowbotham, and D. Maddy (2004), Pliocene and Quaternary regional uplift in western Turkey: The Gediz River terrace staircase and the volcanism at Kula, *Tectonophysics*, *391*(1–4), 121–169, doi:10.1016/j.tecto.2004.07.013.

Whipple, K. X., and C. R. Trayler (1996), Tectonic control of fan size: The importance of spatially variable subsidence rates, *Basin Res.*, *8*, 351–366, doi:10.1046/j.1365-2117.1996.00129.x.

Whipple, K. X., G. Parker, C. Paola, and D. Mohrig (1998), Channel dynamics, sediment transport, and the slope of alluvial Fans: Experimental study, *J. Geol.*, *106*, 677–693, doi:10.1086/516053.

Whitaker, C. R. (1979), The use of the term 'pediment' and related terminology, *Z. Geomorphol.*, *23*, 427–439.

Willett, S. D., S. W. McCoy, J. T. Perron, L. Goren, and C. Y. Chen (2014), Dynamic reorganization of river basins, *Science*, *343*, 1248765, doi:10.1126/science.1248765.

Wilson, L. F., F. J. Pazzaglia, and D. J. Anastasio (2009), A fluvial record of active fault-propagation folding, Salsomaggiore anticline, northern Apennines, Italy, *J. Geophys. Res.*, *114*, B08403, doi:10.1029/2008JB005984.

Yildirim, C., et al. (2013), Tectonic implications of fluvial incision and pediment deformation at the northern margin of the Central Anatolian Plateau based on multiple cosmogenic nuclides, *Tectonics*, *32*, 1107–1120, doi:10.1002/tect.20066.